eNeuro

*Research Article: New Research | Disorders of the Nervous System*

# Role of Endoplasmic Reticulum Stress in Learning and Memory Impairment and Alzheimer's Disease-like Neuropathology in the PS19 and APP$^{Swe}$ Mouse Models of Tauopathy and Amyloidosis

## ER stress in models of tauopathy and amyloidosis

**Denise Isabelle Briggs[1], Erwin Defensor[1], Pooneh Memar Ardestani[1], Bitna Yi[1], Michelle Halpain[1], Guy Seabrook[2] and Mehrdad Shamloo[1]**

[1]*Department of Neurosurgery, Stanford University School of Medicine, 1050 Arastradero Road, Building a, Palo Alto, California 94304-5593*

[2]*California Innovation Center, Johnson & Johnson, 99 El Camino Real, Menlo Park, California 94025*

DOI: 10.1523/ENEURO.0025-17.2017

Received: 20 January 2017

Revised: 4 June 2017

Accepted: 17 June 2017

Published: 5 July 2017

**Author Contributions:** MS and GS designed research; ED, PMA, BY, DIB, and MH performed research; ED and DIB analyzed data; DIB wrote the paper.

**Funding:** Johnson & Johnson
Innovation Grant

**Conflict of Interest:** Authors report no conflict of interest.

This research was supported by a Johnson & Johnson Innovation Grant.

D.I.B. and E.D. contributed equally to the production of this manuscript.

**Correspondence should be addressed to** Mehrdad Shamloo, Department of Neurosurgery, Stanford University School of Medicine,1050 Arastradero Road, Building A, Palo Alto, California, 94304-5593; shamloo@stanford.edu

**Cite as:** eNeuro 2017; 10.1523/ENEURO.0025-17.2017

**Title:** Role of endoplasmic reticulum stress in learning and memory impairment and Alzheimer's disease-like neuropathology in the PS19 and APP$^{Swe}$ mouse models of tauopathy and amyloidosis

**Abbreviated Title:** ER stress in models of tauopathy and amyloidosis

**Author Names:** Denise Isabelle Briggs, PhD[1§], Erwin Defensor, PhD[1§], Pooneh Memar Ardestani MD[1], PhD[1], Bitna Yi, PhD[1], Michelle Halpain, BS[1], Guy Seabrook, PhD[2], Mehrdad Shamloo, PhD[1*]

**Author Affiliation:** [1]Department of Neurosurgery, Stanford University School of Medicine, 1050 Arastradero Road, Building A, Palo Alto, California, 94304-5593

[2]California Innovation Center, Johnson & Johnson, 99 El Camino Real, Menlo Park, California, 94025

[*]Corresponding author at: Department of Neurosurgery, Stanford University School of Medicine,1050 Arastradero Road, Building A, Palo Alto, California, 94304-5593; shamloo@stanford.edu.

[§]Authors contributed equally to the production of this manuscript.

**Author Contributions:** MS and GS designed research; ED, PMA, BY, DIB, and MH performed research; ED and DIB analyzed data; DIB wrote the paper.

**Number of Figures:** 10

**Number of Tables:** 4

**Number of Multimedia:** 0

**Number of words for Abstract:** 246

**Number of words for Significance Statement:** 119

**Number of words for Introduction**: 727

**Number of words for Discussion**: 1901

**Acknowledgements:** We would like to especially acknowledge Dr. Gregor Macdonald as well as the analytical chemistry team in Janssen, Beerse, Belgium for their support with the analysis and structure confirmation of ISRIB used in these studies. We would like to thank Dr. Andrew Evans for his insight and intellectual contribution in reviewing our manuscript. We would like to

5 thank Stanford behavioral and functional neuroscience laboratory (SBFNL: NINDS **P30** center
6 core grant: NS06937 501A1) for conducing all behavioral and pharmacological experiments in
7 this report.
**Conflict of Interest:** Authors report no conflict of interest.

**Sources of support:** This research was supported by a Johnson & Johnson Innovation Grant.

## ABSTRACT

Emerging evidence suggests that endoplasmic reticulum (ER) stress may be involved in the pathogenesis of Alzheimer's disease (AD). Recently, pharmacological modulation of the Eukaryotic Initiation Factor 2-alpha (eIF2α) pathway was achieved using an Integrated Stress Response Inhibitor (ISRIB). While members of this signaling cascade have been suggested as potential therapeutic targets for neurodegeneration, the biological significance of this pathway has not been comprehensively assessed in animal models of AD. The present study investigated the ER stress pathway and its long-term modulation utilizing *in vitro* and *in vivo* experimental models of tauopathy (MAPT P301S)PS19 and amyloidosis ($APP^{Swe}$). We report that thapsigargin induces activating transcription factor 4 (ATF4) in primary cortical neurons (PCNs) derived from rat and $APP^{Swe}$ non-transgenic and transgenic mice. ISRIB mitigated the induction of ATF4 in PCNs generated from wild-type but not $APP^{Swe}$ mice despite partially restoring thapsigargin-induced translational repression in non-transgenic PCNs. *In vivo*, C57BL/6J and PS19 mice received prolonged, once-daily administration of ISRIB. While the compound was well tolerated by PS19 and C57BL/6J mice, $APP^{Swe}$ mice treated per this schedule displayed significant mortality. Thus, the dose was reduced and administered only on behavioral test days. ISRIB did not improve learning and memory function in $APP^{Swe}$ transgenic mice. While ISRIB did not reduce tau-related neuropathology in PS19 transgenic mice, no evidence of ER stress-related dysfunction was observed in either of these transgenic models. Taken together, the significance of ER stress and the relevance of these models to the etiology of AD require further investigation.

## SIGNIFICANCE STATEMENT

Accumulating evidence suggests that endoplasmic reticulum (ER) stress is involved in cellular processes relevant to neuronal survival and death in disorders of the CNS. We assessed the ER stress pathway and the effects of its modulation utilizing *in vitro* and *in vivo* experimental models of tauopathy and excessive amyloidosis. Use of an Integrated Stress Response Inhibitor (ISRIB) was not effective at improving the behavioral impairments and neuropathology observed in these models. While no evidence of ER stress or ER stress-related dysfunction involving ATF4 and CHOP was found in these transgenic mice, ISRIB partially restored thapsigargin-induced translational repression *in vitro* in primary mouse cortical neurons. In summary, the contribution of ER stress to the etiology of AD warrants further investigation.

## INTRODUCTION

Alzheimer's disease (AD) is a progressive, neurodegenerative disorder characterized by memory loss and global cognitive decline (Alzheimer's, 2013). The neuropathological hallmarks of AD include neuronal loss (Terry et al., 1991) accumulation of extracellular Aβ plaques, and neurofibrillary tangles composed of intracellular aggregates of tau protein (Selkoe, 2001; Schoonenboom et al., 2004; Sobow et al., 2004; Iqbal et al., 2005). Over 46 million people worldwide are currently living with AD or some form of dementia (Prince M, 2015). This number is expected to exceed 130 million by the year 2050 (Prince M, 2015). Presently, all approved treatments for AD are geared toward symptom management and do not target the underlying neuropathology. Despite the pressing need for more targeted treatments, to date, all phase III clinical trials testing therapeutics directed at the neuropathological substrates of AD have failed (Mullane and Williams, 2013; Gauthier et al., 2016). This has intensified the investigation of alternative therapeutic targets implicated in the pathogenesis of AD.

Emerging evidence suggests that endoplasmic reticulum (ER) stress may play an integral role in the development of AD (Paschen and Mengesdorf, 2005a, b; Lindholm et al., 2006; Hoozemans et al., 2009; Scheper and Hoozemans, 2009). A fundamental role of the ER is to ensure that newly synthesized proteins are folded correctly. An aberrant accumulation of unfolded proteins activates multiple signaling pathways collectively referred to as the unfolded protein response (UPR) (Spatara and Robinson, 2010). Markers of the UPR have been detected postmortem in the brain tissue of AD patients (Hoozemans et al., 2005; Scheper and Hoozemans, 2015) and UPR activation has been correlated with tau phosphorylation, a critical step preceding the formation of neurofibrillary tangles (Hoozemans et al., 2009). The protein kinase R (PKR)-like ER kinase (PERK), along with inositol-requiring protein 1, and activating transcription factor-6, are three classes of sensors that recognize unfolded proteins in the ER (Schroder and Kaufman, 2005). In response to ER stress, PERK becomes activated via

dimerization and autophosphorylation (Harding et al., 1999; Marciniak et al., 2006) and the collective response of these pathways is referred to as the Integrated Stress Response (ISR) (Wek et al., 2006; Sidrauski et al., 2013). Upon activation, PERK phosphorylates the α-subunit of eukaryotic translation initiation factor-2 (eIF2α) (Harding et al., 2000) allowing it to complex with and de-activate eIF2B (elongation initiation factor 2 B). With few exceptions, this inhibits global protein synthesis and can alleviate ER stress by preventing further accumulation of unfolded proteins. One exception is the stress-related mRNA activating transcription factor-4 (ATF4), whose translational efficiency is up-regulated by phosphorylation of eIF2α (Harding et al., 2000; Ameri and Harris, 2008). While ATF4 induction can promote the synthesis of pro-survival ER chaperone proteins (Li et al., 2008), it is also a potent inducer of C/EBP-homologous protein (CHOP), a pro-apoptotic transcription factor whose expression is increased under severe or persistent ER stress (Marciniak et al., 2004; Lenna and Trojanowska, 2012).

Previous studies identified a small molecule Integrated Stress Response Inhibitor (ISRIB) that targeted selective components of the ER stress pathway and may afford a safer and more tolerable means of target engagement than direct PERK inhibition. ISRIB was reported to improve learning and memory performance in healthy, wild-type (WT) rodents (Sidrauski et al., 2013). *In vitro*, ISRIB mitigated the induction of ATF4 in HEK293 cells challenged with the ER stress inducers thapsigargin and tunicamycin (Sidrauski et al., 2013). Recently, the mechanism by which ISRIB exerts its modulatory control was identified (Sidrauski et al., 2015a). EIF2B dimerizes in response to ER stress, and ISRIB was found to bind and stabilize activated eIF2B dimers, thereby diminishing their sensitivity to eIF2 phosphorylation (Sidrauski et al., 2015b) and lifting the inhibition of protein translation resulting from phosphorylation of eIF2α (Sekine et al., 2015; Sidrauski et al., 2015a; Sidrauski et al., 2015b).

While modulation of eIF2 phosphorylation using ISRIB was found to abate the effects of ER stress *in vitro*, few studies have investigated if ER stress-related dysfunction could be

89 targeted to improve AD-like outcomes *in vivo*. To our knowledge, this is the first study to
90 investigate the role of ER stress and the effects of long-term ISR-related pharmacological
91 modulation on AD-like neuropathology and behavior both *in vitro* and *in vivo*. Specifically, the
92 studies described herein assessed the ER stress pathway and the effects of ISRIB treatment *in*
93 *vitro* using PCNs and *in vivo* utilizing experimental AD models of tauopathy (MAPT P301S)PS19
94 (PS19) and excessive amyloidosis ($APP^{Swe}$).

## MATERIALS AND METHODS

### Primary neuronal culture

Primary cortical neurons (PCNs) derived from E17 Sprague-Dawley rats (Charles River Laboratories), E18 $APP^{Swe}$ transgenic (Tg) and non-transgenic (nTg) mice (Taconic1349, Tg2567), and C57Bl/6N mice (Charles Rivers Laboratories) were dissociated by incubating cortical tissue in 2 mL of Hibernate E medium (BrainBits, Springfield, IL) without calcium containing 4 mg papain (Worthington Biochemical, Lakewood, NJ) at 37°C for 30 min. Further dissociation was accomplished by trituration using a fire-polished Pasteur pipette (Thermo Fisher, Waltham, MA). The supernatant was centrifuged (CL2, Thermo Fisher, Waltham, MA) at 1100 rpm for 1 min and the cell pellet suspended in 2 mL of serum-free MB Activ1l medium (BrainBits, Springfield, IL) supplemented with an antibiotic solution of penicillin (100 U/ml; Invitrogen, Carlsbad, CA) and streptomycin (100 mg/ml; Invitrogen, Carlsbad, CA). Cells were counted and seeded onto poly-D-Lysine (Sigma-Aldrich, St. Louis, MO) coated plates. Cells were plated at a density of $1.0 \times 10^6$ or $1.5 \times 10^6$ cells per well in 6-well plates, and $8 \times 10^4$ cells per well in 96-well plates. PCNs isolated from rats were cultured for 12–13 days in vitro (DIV), and PCNs isolated from $APP^{Swe}$ mice were cultured for 7, 11, or 13 DIV.

### Chemicals

Thapsigargin and puromycin were obtained from Sigma-Aldrich (St. Louis, MO) and the trans-isomer of ISRIB from Selleck Chemicals (SKU S7400, Houston, TX). The physical and chemical properties of ISRIB were analyzed using high performance liquid chromatography and nuclear magnetic resonance spectroscopy and found to be consistent with those previously reported (analysis by Selleck Chemicals). http://www.selleckchem.com/products/isrib-trans-isomer.html.

### Target engagement and ER stress *in vitro*

To induce ER stress, PCNs were cultured in 6-well plates as described above and incubated for 4 h with 1 μM thapsigargin, 1 μM thapsigargin + 200 μM ISRIB, or DMSO ((dimethyl sulfoxide),

Sigma-Aldrich, St. Louis, MO), which served as a vehicle control. To evaluate the effects of ISRIB on protein synthesis, the SUnSET technique was used as previously described by Schmidt and colleagues (Schmidt et al., 2009). PCNs isolated from C57Bl/6N mice were cultured for 7 or 11 DIV and challenged with thapsigargin or thapsigargin + ISRIB as described above. Ten minutes prior to collection, cells were treated with puromycin (10 µg/ml).

*Immunoblotting*

PCNs were washed with 1x PBS (Thermo Fisher, Waltham, MA) and lysed in M-PER Tissue Protein Extraction Reagent (Life Technologies, Carlsbad, CA) with Mini Complete Protease Inhibitor tablet (Roche, Basel, Switzerland). Samples were homogenized on ice using an Ultrasonic Probe Homogenizer (Omni International, Kennesaw, GA) and centrifuged at 15,000 x g for 10 min at 4°C. The supernatants were collected and stored as the soluble fraction. Protein concentration was determined using the BCA protein assay kit (Pierce, Rockford, IL). Samples were boiled, loaded (40 µg/well) and resolved by 14% Tris-Glycine SDS-PAGE (Life Technologies, Carlsbad, CA) electrophoresis under reducing conditions. The protein was transferred to a polyvinylidene difluoride membrane (Life Technologies, Carlsbad, CA) and incubated in blocking buffer (0.05% Tween-20, Sigma-Aldrich, St. Louis, MO; 2% normal goat serum, Sigma-Aldrich, St. Louis, MO; 5% non-fat milk, Biorad, Hercules, CA); 1x TBS, Promega, Madison, WI) for 1 h at room temperature. Primary antibodies directed at ATF4 (1:300, Santa Cruz Bio, sc-200), CHOP (1:300, Santa Cruz Biotechnology, Santa Cruz, CA), puromycin clone 12D10 (1:10,000; EMD Millipore, Hayward, CA), tubulin (1:300, Sigma-Aldrich, St. Louis, MO), and GAPDH (glyceraldehyde 3-phosphate dehydrogenase; 1:5000; Sigma-Aldrich, St. Louis, MO) were incubated at 4°C either overnight (ATF4, CHOP, puromycin) or for 30 min (tubulin, GAPDH). The following day, membranes were washed (3 x 5 min) with 0.05% Tween-20 in 1x TBS and incubated for 1 h with the appropriate HRP-conjugated secondary antibody (goat anti-mouse, goat anti-rabbit; 1:5000, Life Technologies, Carlsbad, CA). Membranes were incubated

briefly in ECL substrate (SuperSignal West Dura, Thermo Fisher, Waltham, MA) and exposed to film (Konica Minolta, Tokeyo, Japan) for protein detection. ImageJ software (NIH) was used for densitometry analysis of protein levels and expression levels normalized to internal control.

*Lactate dehydrogenase (LDH) cytotoxicity assay*

The LDH assay was conducted according to the manufacturer's protocol (Thermo Fisher, Waltham, MA). PCNs isolated from E17 rat embryos were cultured in 96-well plates (Thermo Fisher, Waltham, MA) as described above. Cells were treated with 10 μM thapsigargin, 10 μM thapsigargin + 200nM ISRIB, 10 μM thapsigargin + 1 μM ISRIB, DMSO vehicle control, or DMSO vehicle control + lysis buffer (positive control) and incubated for 48 h. The media was collected and each sample transferred to a 96-well plate (50 μl/well). The reaction solution was added and allowed to incubate for 30 min. The stop solution was added and the absorbance read between 490 and 680 nm using a Flex Station 3 microplate reader (Molecular Devices, Sunnyvale, CA). Percentage cytotoxicity was calculated by subtracting LDH activity of the negative vehicle control from the LDH activity of thapsigargin-treated samples. This value was then divided by the total LDH activity [(maximum LDH release control activity) – (negative control activity)], and multiplied by 100.

**Animals**

All animal procedures were performed in accordance with the Stanford University animal care committee's regulations. The studies described herein were conducted in compliance with all applicable sections of the current version of the Final Rules of the Animal Welfare Act Regulations (9 CFR) and the Guide for the Care and Use of Laboratory Animals, Institute of Laboratory Animal Resources, Commission on Life Sciences, National Research Council, 2010. Animals were housed at a standard temperature (22 ± 1°C), in a reverse-cycle light-controlled environment (lights on from 8:30 pm to 8:30 am) with *ad libitum* access to food and water. A summary of the mice used for the present studies is provided in **Table 1**. A total of 194 male

mice were used for this study including 3-month old male C57BL/6J mice (N=20, Jackson Laboratory, stock #0664), 5-month-old male C57BL/6J mice (N=12), 8 to 9-month-old male PS19 mice (N=102, Jackson Laboratories, stock #8169, B6;C3-Tg (Prnp-MAPT*P301S)PS19Vle/J), and 5 to 6-month-old male $APP^{Swe}$ mice (N=60, Taconic, stock # 1349, B6;SJL-Tg(APPSWE)2576Kha). Two separate cohorts of PS19 mice were used for our studies. Each cohort was age-matched and subjected to the same treatment regimen and behavioral testing schedule. The results from each cohort were pooled for our statistical analysis. One C57BL/6J mouse + ISRIB developed irritation at the injection site during the ninth week of treatment and was sacrificed. In the combined PS19 cohorts, a total of 3 nTg mice + vehicle died over the course of the behavioral experiments. One mouse died in the third week and 2 mice died in the fifth week. One nTg mouse + ISRIB died in the fifth week. A total of 8 PS19 Tg mice + vehicle died. One mouse died in the first week, 6 mice died in the fifth week and 1 mouse died in the sixth week. A total of 6 PS19 Tg mice + ISRIB died. One mouse died in the second week, 1 mouse died in the third week, 3 mice died in the fifth week and 1 mouse died in the sixth week. A total of 7 $APP^{Swe}$ mice died during the second week of treatment: 4 nTg mice + ISRIB and 3 Tg mice + ISRIB.

**ISRIB preparation and dosing *in vivo***

ISRIB was delivered via intraperitoneal (IP) injection in a vehicle consisting of 5% PEG400 (EMD Millipore, Billerica, MA) and 5% Tween20 in 1x PBS. To prepare the test article for dosing, ISRIB was weighed out and placed in a 50 mL conical. Appropriate volumes of PEG400, Tween20, and water were added followed by sonication on ice using a probe homogenizer. PBS followed by water was added to the solution to achieve a stock concentration of 0.5 mg/ml. The stock was further diluted to achieve concentrations of 0.25 mg/ml and 0.025 mg/ml. Based on an administration volume of 10 mL/kg, the administrative doses of ISRIB were 5 mg/kg, 2.5 mg/kg, and 0.25 mg/kg, respectively. Dosing solutions were prepared fresh daily, protected from light,

and used within 24 h. Body weight and pre-dose activity chamber parameters were used to pseudo-randomize and balance treatment groups prior to the start of treatment. C57BL6/J and PS19 mice received a single daily injection of either vehicle or ISRIB (5 mg/kg) for 9 weeks. Over the course of treatment, PS19 mice underwent behavioral testing. $APP^{Swe}$ Tg and nTg mice received a single daily dose of either vehicle or ISRIB (5 mg/kg) on days 1 through 8. In $APP^{Swe}$ mice, daily administration was stopped due to a significant increase in mortality in all mice treated with ISRIB. For the remainder of the study, the dose was reduced and administered only on behavioral test days as follows: vehicle or ISRIB (2.5 mg/kg) 1 h before testing in the Y-Maze, vehicle or ISRIB (0.25 mg/kg) immediately after the last trial of the day in the Morris water maze (MWM), and vehicle or ISRIB (2.5 mg/kg) 1 h before the novel object recognition (NOR) and novel object location (NOL) tests. Previous research found that a single dose of ISRIB enhanced behavioral function in healthy, WT mice (Sidrauski et al., 2013). This research informed our decision to modify our paradigm for the remainder of the study and dose only on behavioral test days at the concentrations described above.

**ISRIB pharmacokinetics and tolerability**

C57BL/6J mice ~3 months old received a single IP injection of either vehicle or ISRIB (5 mg/kg). Brain and plasma were collected at 5 different time points following the injection (immediately, 0.5 h, 2 h, 4 h, and 8 h after the injection). All animals were anesthetized using isoflurane (Butler Animal Health Supply, Dublin, OH) gas and euthanized per [Author University] APLAC Guidelines. Blood was collected by transcardial puncture and transferred to plasma separation tubes containing lithium heparin (Becton Dickenson, East Rutherford, NJ). Tubes containing blood were centrifuged at 4°C at 15,000 x g for 2 min. Plasma was transferred to separate microfuge tubes and stored at -80°C. Mice were perfused with 1x PBS using a low perfusion flow rate to avoid bursting vessels (1-2 on Variable Flow Minipump by VWR). Mice were decapitated and whole brains extracted, frozen on dry ice, and stored at -80°C. Frozen brain tissues were

weighed and two volumes of Milli Q water added. Tissues were homogenized on ice using an ultrasonic probe homogenizer. For spiked standards, 25 µl of ISRIB was added to 25 µl of brain tissue homogenate or plasma. For samples, 25 µl of 50% methanol (Fisher Scientific, Hampton, NH) was used in place of standards. Next, 150 µl of acetonitrile (Fisher Scientific, Hampton, NH)/methanol 80:20 (v/v) was added to the mixture, vortexed vigorously for 1 min, and centrifuged at 3,000 x g for 5 min. The supernatant was diluted with water (1:1) and the concentrations of ISRIB in brain and plasma determined using liquid chromatography tandem mass spectrometry. Liquid chromatography separation was carried out on a C18 column (50 mm × 2.1 mm, 5 µm; Thermo Fisher, Waltham, MA) with isocratic elution using a mobile phase composed of water and acetonitrile. Formic acid (0.1%; Fisher Scientific, Hampton, NH) was added to both aqueous and organic phases. The column temperature was set to 25ºC and the injection volume was 10 µl. The mass spectrometer was operated in the positive mode with multiple-reaction monitoring. Multiple-reaction monitoring transition of 451.1→266.0 was used as the quantifier and 451.1→141.0 was used as the qualifier. Data acquisition and analysis were performed using the Analyst 1.6.1 software (AB SCIEX, Framingham, MA). To ensure mice could tolerate prolonged once daily treatment, C57BL/6J mice ~5 months old were administered either vehicle or ISRIB (5 mg/kg) once daily for 62 consecutive days. Body weight was recorded weekly and notable observations, if any, were recorded daily. Upon completion of this preliminary study using WT mice, *in vivo* and *in vitro* experiments using PS19 and $APP^{Swe}$ mice were conducted in parallel.

**Behavioral assessment**

One experienced researcher was assigned to conduct all behavioral tests and remained blinded to the experimental groups throughout the entire in-life phase of the study. Groups were pseudo-randomized using baseline activity chamber performance and body weight as previously stated. Unless otherwise noted, all animals were habituated to the testing area for at least 1 hour prior to

testing. Except for the water maze and unless otherwise noted, all apparatuses were cleaned with 1% Vikron solution between subjects. A timeline of the behavioral studies and treatment schedule is provided in **Fig. 1**.

***Locomotor activity***

Locomotor activity was measured in an activity arena (43 cm l x 43 cm w x 30 cm h; Med Associates Inc., St. Albans, VT) equipped with three planes of infrared detectors inside a sound-attenuating chamber (74 cm l x 60 cm w x 60 cm h; Med Associates Inc., St. Albans, VT). Each subject was placed in a corner of the arena and allowed to move freely for 10 min. During that time, activity was recorded using a computer-interfaced infrared beam tracking system (Activity Monitor software V5.93.773; Med Associates Inc., St. Albans, VT). Total activity was defined as the sum of all beam breaks in both the horizontal and vertical planes throughout the entire session. Dependent variables included ambulatory distance, ambulatory duration, ambulatory velocity, time spent in pre-defined zones, and the number and/or frequency of jumping and rearing. Following the first day of treatment, PS19 mice were tested on days 4, 11, 18, and 25 (see **Fig. 1**) and $APP^{Swe}$ mice were tested on day 7.

***Anxiety-like behavior***

The elevated plus maze (EPM) was used to assess anxiety-like behavior. The EPM apparatus (custom built) consists of two open arms (30 cm l x 5 cm w, with a 0.3 cm h lip around the edges) and two closed arms (30 cm l x 5 cm w x 15 cm h) that extend from a common center (5 cm x 5 cm). The maze was elevated 63 cm above the floor and the light intensity adjusted to ~7 lux. Each mouse was gently placed in the center of the maze facing away from the investigator and allowed to move freely for 5 min. Movement was recorded using a WV-CP484 camera (Panasonic Corporation, Osaka, Japan) and a computer-interfaced video tracking system (EthoVision XT, version 8.1; Noldus, Leesburg, VA). Dependent variables included the total number of arm entries and time spent in each arm. PS19 mice were tested on day 22.

***Learning and memory outcomes***

*Fear conditioning*

Fear conditioning was used to assess fear-associative learning and recall. Mice were placed in the fear-conditioning chamber (Coulbourne Instruments, Whitehall, PA) for 120 s. After 120 s, a 15 s tone (1700 Hz, 80 dB) was presented. A shock (1.5 mA) was delivered during the last 2 s of the tone. After 120 s, the tone and shock were presented again and 30 s later, mice were removed from the chamber. Contextual and cued retrieval testing occurred 24 h after completion of fear conditioning. To assess context retrieval, mice were placed back in the fear-conditioning chamber for 300 s and the time spent freezing was recorded and analyzed using FreezeFrame software V2.10 (Coulbourne Instruments, Whitehall, PA). Freezing was defined as the complete absence of movement lasting ≥ 0.75 s. Cued retrieval was assessed 1 h following the completion of contextual retrieval testing. Mice were placed in an unfamiliar context containing different tactile, spatial and olfactory cues for 180 s. After 180 s, mice were presented with a tone (1700 Hz, 80 dB) lasting 180 s and time spent freezing was recorded. The dependent variable of percent time spent freezing was used as an index of fear-based learning and memory. $APP^{Swe}$ mice were tested on days 1 and 2.

*Y-maze*

The Y-maze (custom built) was used to assess spontaneous alternation, an exploratory behavior displayed by rodents. The maze is comprised of 3 arms arranged at 120° angles. Two of the arms are of equal length (15.24 cm x 12.7 cm x 7.62 cm) and one arm is longer (20.32 cm x 12.7 cm x 7.62 cm). Each mouse was placed in the maze facing away from the center and allowed to move freely for 5 min. Scoring was conducted in real time through live video feed (Roxio adaptor, Santa Clara, CA; WV-CP484 camera, Panasonic Corporation, Osaka, Japan). Dependent variables including sequence and total number of arm entries were recorded for each mouse. Entry was defined as having all 4 limbs inside the arm. Alternation was defined as any sequence

of 3 unique arms entries (i.e. “ABC,” “BAC,” but not “CAC”). The percent alternation rate was calculated as follows: number of alternations/total number of possible alternations*100 and compared to 50% chance alternation. $APP^{Swe}$ mice were tested on day 14.

*Morris water maze*

The MWM was used to assess spatial learning and memory. The maze consists of a round polyethylene tank (172 cm diameter) filled with water. During training, a platform is submerged 1 cm below the water surface. Tempura paint is added to the water until it becomes opaque and the platform no longer visible. Visual cues are mounted to privacy blinds surrounding the maze. The temperature of the testing room and water was approximately 21°C. Movement of the subject was recorded using a computer-interfaced video tracking system (EthoVision XT, version 8.1; Noldus, Leesburg, VA) and the output used for our analysis. Dependent variables included thigmotaxis, swim velocity, latency to locate the platform, and time spent in the target and nontarget zones. The target zone describes the zone that originally housed the platform. The protocol was modified for PS19 and $APP^{Swe}$ mice as described below.

*MWM protocol for PS19 mice*

*Pre-training*: Pre-training occurred in a single day and consisted of 4 consecutive trials per mouse. Mice were placed in the maze at the end of a rectangular channel (22 cm x 172 cm) that led to the platform (22 $cm^2$). The drop location alternated between the two short sides of the rectangular channel. Mice were required to locate, climb, and remain atop the platform for 3 s. *Hidden platform training*: Two training sessions were conducted per day for 5 days. Each session consisted of two 90-s trials. The inter-session interval was 3-4 h and the inter-trial interval was 20-30 min. Pseudo-randomized drop locations were scheduled for each subject in all remaining phases of the test. Each mouse was placed in the maze and allowed to swim freely until they located the platform or the trial ended. Mice that failed to locate the platform were gently guided to its location by the experimenter. Latency to locate the platform was recorded.

*Probe test*: To assess spatial memory recall, probe tests were conducted 24 h and 72 h following completion of hidden platform training. During the probe test, the platform was removed and mice were allowed to swim freely for 90 seconds. The number of visits to the zone that originally housed the platform (target zone) and time spent in the target and nontarget zones was recorded. *Visible platform training*: Visible platform training occurred in a single day and consisted of 4 trials. The platform was returned to a new location indicated by a ping-pong ball atop a mast. Each mouse was placed in the maze and allowed to swim freely for the duration of each 90-second trial. Latency to locate the platform was recorded. PS19 mice underwent pre-training on day 28 and hidden platform training on days 29 - 33. The 24 h probe test was administered on day 34, and the 72 h probe test was administered on day 36. Visible platform training occurred on day 39.

*MWM protocol for APP$^{Swe}$ mice*

General procedures for the MWM were conducted as described above with the following modifications. *Pre-training:* The channel used in the pre-training phase measured 17 cm x 172 cm and contained a 17 cm$^2$ platform. *Hidden & visible platform training:* The 17 cm$^2$ platform was used on days 1 and 2 of hidden platform training and a 22 cm$^2$ platform was used on day 3. Hidden platform training was terminated after 4 days due to learning failures across all groups. Five days later, visible platform training was conducted using the 22 cm$^2$ platform and took 3 days to complete. The following day, hidden platform training resumed and lasted for 5 days. Training was conducted in a single session comprised of 4 trials each day. Each trial was 120 seconds long separated by an inter-trial interval of 35-45 min. The following and final day of testing consisted of a single probe trial followed by 4 reversal trials. Reversal trials were conducted by moving the platform to a new location. APP$^{Swe}$ mice underwent pre-training on day 28 and hidden platform training on days 29 - 32. The first round of hidden platform training was terminated because mice failed to acquire the task. APP$^{Swe}$ mice underwent visible platform

345 training on days 41-43. Hidden platform training resumed and occurred on days 44-48. The 24 h
346 probe test was administered on day 49, followed that same day by 4 reversal trials.

347 *Passive avoidance*

348 The passive avoidance (PA) test was used to assess fear-based learning and memory. The PA
349 chamber (GEMINI$^{TM}$ system, San Diego Instruments, San Diego, CA) consists of a lighted and
350 dark compartment separated by an automated guillotine-style door (gate). Both compartments
351 have a grid floor equipped to deliver electrical shocks. Each mouse was placed into the lighted
352 compartment to habituate to the apparatus. After 30 s, the gate opened allowing access to the
353 dark compartment. As soon as the mouse entered the dark compartment, the gate closed. The
354 following day, mice were placed into the lighted compartment. After 30 s, the gate opened
355 allowing access to the dark compartment. Once the subject crossed into the dark compartment,
356 the gate closed. Following a 3 s delay, a 0.65 mA shock was delivered for 2 s. The following day,
357 mice were again placed into the lighted compartment. After 5 s, the gate opened allowing access
358 to the dark compartment and closed upon entry. The dependent variable of latency to enter the
359 dark compartment was recorded and used as an index of fear-based memory. PS19 mice were
360 tested on days 46 − 48.

361 *Novel object location and novel object recognition*

362 To assess recognition memory, mice were tested using the novel object location (NOL) and
363 novel object recognition (NOR). The NOL task assesses the ability of a subject to detect that a
364 familiar object has been moved to a new location. The NOR task assesses the ability of a subject
365 to detect that a familiar object has been replaced with a novel object. Testing occurred in a
366 plastic arena (52 cm w x 52 cm l x 40 cm h) with a white floor, black walls, and a white card fixed
367 to one wall. The placement of the objects as well as the object replaced was pseudo-randomized
368 across subjects. On the first day, mice were habituated to the testing arena and allowed to
369 explore freely for 10 min. The following day, the NOL test was conducted. Mice were placed in

the center of the arena containing three identical objects, each placed in a corner, 10 cm from the wall. Mice were then returned to the homecage for 3-4 min. During that time, one of the objects was moved to the previously empty corner. Mice were placed back in the center of the arena and allowed to explore freely for 10 min. Time spent investigating the novel or familiar location was recorded using a computer-interfaced video tracking system (EthoVision XT, version 8.1; Noldus, Leesburg, VA) and the output used for our analysis. For the NOR test, mice were placed in the center of the arena containing three identical objects, each placed in a corner, 10 cm from the wall. Mice were returned to their homecage for 3−4 min. During that time, one of the familiar objects was replaced with an unfamiliar object. Mice were again placed in the center of the arena and allowed to explore freely for 10 min. Time spent investigating the novel or familiar object was recorded. $APP^{Swe}$ mice were tested over days 69 − 74.

**Exclusions & criteria**

Mice exhibiting signs of locomotor impairment, potential blindness, or poor health were excluded from all behavioral tests. During the NOL and NOR tests, mice that traveled < 1000 cm during the test trial were excluded from analysis. Mice who met any of the following criteria during the MWM were excluded from our analyses: 1) exhibiting > 85% (~ 77 s) thigmotaxis in all visible or hidden platform trials; 2) failure to locate the platform in > 50% of all visible platform trials; 3) failure to display learning during hidden platform trials.

**Target engagement *ex vivo***

*Immunoblotting*

Upon completion of behavioral testing, mice were sacrificed and their brains were removed. The left and right hemispheres were divided sagittally along the midline. One hemisphere was placed in neutral buffered formalin (VWR, Radnor, PA) for immunohistochemistry and the other was frozen on dry ice for analysis by western blot. Frozen brain tissues were homogenized in RIPA buffer (Thermo Fisher, Waltham, MA) containing protease and phosphatase inhibitor cocktails.

Lysates were centrifuged (Sorvall Legend, Thermo Fisher, Waltham, MA) at 4°C at 10,000 x g for 15 min. Supernatants were collected and protein was quantified by the BCA assay. Equal amounts of protein (60, 6, or 10 µg) were resolved by SDS-PAGE and transferred onto a polyvinylidene difluoride (Life Technologies, Carlsbad, CA) membrane. Primary antibodies directed against ATF4 (1:300, Santa Cruz Bio, sc-200), CHOP (1:300, Santa Cruz Bio, sc-575), AT8 (1:200, Pierce, Rockford, IL); Tau-5 (1:200, Abcam, Cambridge, UK); GAPDH (1:5000; Sigma-Aldrich, St. Louis, MO) and tubulin (1:300; Sigma-Aldrich, St. Louis, MO) were incubated at 4°C overnight except GAPDH and tubulin, which were incubated for 1 h or 30 min, respectively. Membranes were then washed (3 x 5 min) with 0.05% tween-20 in 1x PBS, and incubated with the appropriate HRP-conjugated secondary antibody. Signal was detected using SuperSignal West Dura Extended Duration Substrate (Thermo Fisher, Waltham, MA) and the membranes exposed to film. The integrated density of proteins was quantified using ImageJ software (NIH) and normalized to the appropriate internal control.

*Immunohistochemistry*

Brain tissue was post-fixed in formalin for 24 h and transferred to 30% sucrose (Sigma-Aldrich, St. Louis, MO). After saturation in sucrose, brains were frozen in isopentane (Sigma-Aldrich, St. Louis, MO) on dry ice and stored at -80°C. Brains were sectioned coronally at 40 µm and stored at -20°C in cryoprotectant (20% glycerol, 30% ethylene glycol in phosphate buffer). Floating sections were washed in 1x PBS and blocked for 90 min at room temperature in 1x PBS containing 3% bovine serum albumin (Sigma-Aldrich, St. Louis, MO) and 0.3% Triton X-100 (Sigma-Aldrich, St. Louis, MO). Sections were incubated in primary antibody AT8 (1:300, Pierce, Rockford, IL) in 1x PBS containing 1% bovine serum albumin and 0.1% Triton X-100 at room temperature overnight and then washed with 1x PBS (3 x 15 min). Sections were incubated in fluorescent red fluorescent Nissl stain for 20 min (1:100, Life Technologies, Carslbad, CA) and/or secondary antibody (488 donkey anti mouse, 1:250, Jackson ImmunoResearch, West Grove,

PA) with DAPI nuclear stain (1:5000; Sigma-Aldrich, St. Louis, MO) for 1.5 h in 1x PBS. Sections were mounted onto slides coated with 0.15% gelatin and coverslipped with polyvinyl alcohol mounting media containing DABCO antifade (Sigma-Aldrich, St. Louis, MO). Images were acquired on a Zeiss Axio Imager 2 microscope. Image based quantifications were performed on two sections per mouse using ImageJ software (NIH). Hippocampal pyramidal cell layer thickness was quantified from nissl stained images using the ImageJ line tool. Two sections per animal were imaged at 5x magnification and three measurements per region were taken and used for our analysis. AT8 mean staining intensity and inclusion numbers were quantified using the ImageJ freehand selection and count tool. A reviewer blind to treatment group and genotype using images acquired at 40x magnification performed quantification. Two sections per animal were imaged and the average of two measurements per region used for our analysis.

**Data Analysis**

Statistical analysis was performed using GraphPad Prism software (version 6.0b). Statistical tests used for analysis included one-way ANOVA, two-way repeated measures (RM) ANOVA, mixed-measures ANOVA (SPANOVA), paired and unpaired two sample t-test, one sample t-test, linear regression, Mantel-Cox, and two-way ANOVA. To correct for multiple comparisons, Bonferroni's correction was used unless otherwise stated. A summary of the tests used for statistical analysis is provided in **Table 2**. The average for a particular test point was substituted for missing values due to mortality or exclusion for analyses requiring SPANOVA or two-way RM ANOVA. Outliers were identified using extreme studentized deviate method. Statistics for each outcome measure are described in detail in their respective Results section. Statistical significance was defined at the level of $p < 0.05$. For the sake of analyzing phenotype, comparisons were made to nTg vehicle control and the results for PS19 and $APP^{Swe}$ mice are summarized in **Tables 3** and **4**, respectively.

## RESULTS

### ER Stress and target engagement- *in vitro*

*Thapsigargin induces ATF4, CHOP, and cytotoxicity in rat PCNs with partial restoration by ISRIB*

Thapsigargin is a potent ER stress inducer (Thomenius and Distelhorst, 2003; Kim et al., 2008b) that has been successfully used in immortalized cell lines (Sidrauski et al., 2013). ISRIB was previously found to block PERK-mediated induction of ATF4 in HEK293 cells challenged with thapsigargin and tunicamycin (Sidrauski et al., 2013) and CHOP in U2OS cells challenged with tunicamycin (Sidrauski et al., 2013). To investigate the ER stress pathway *in vitro* and to ensure target engagement, PCNs derived from E17 Sprague-Dawley rats were treated with 100 nM or 1 μM thapsigargin. To assess the ability of ISRIB to mitigate these effects, cells were additionally treated with 20 nM or 200 nM ISRIB. While the IC50 of ISRIB-A1 was originally reported at 5 nM (Sidrauski *et al*., 2013), a recent report cited assay-dependent IC50 values of 27-35 nM (Sekine *et al*., 2015). As such, we chose to use a minimally effective dose (20 nM) and one that was ~10-fold above cell-based IC50 values (200 nM). The effects of thapsigargin and ISRIB treatment on the induction of ATF4, CHOP, and cytotoxicity in rat PCNs are shown in **Fig. 2**. The main effect of treatment on levels of ATF4 (one-way ANOVA; $F(2, 12) = 43.91$, $p < 0.0001$) was significant and is shown in **Fig. 2B**. Compared to cells treated with DMSO (vehicle control), cells treated with 1 μM thapsigargin (Bonferroni's MCT, $p < 0.0001$) and 1 μM thapsigargin + 200 nM ISRIB (Bonferroni's MCT, $p = 0.0024$) had higher levels of ATF4. Compared to cells treated with 1 μM thapsigargin, cells treated with 1 μM thapsigargin + 200 nM ISRIB had lower levels of ATF4 (Bonferroni's MCT, $p = 0.0038$). Compared to vehicle control, cells treated with 1 μM thapsigargin ($t(5) = 3.805$, $p = 0.0126$) had significantly higher levels of CHOP as shown in **Fig. 2C**. Cells treated with 1 μM thapsigargin + 200 nM ISRIB also had higher levels of CHOP compared to cells treated with vehicle, though the results were not significant ($p = 0.0824$). While chronic ER stress is known to compromise cell viability and induce apoptosis (Tabas and Ron,

2011; Verfaillie et al., 2013) the role of the PERK- eIF2α pathway in the regulation of cell death is not entirely clear (Kim et al., 2008b). To investigate if any effect of eIF2B-related modulation by ISRIB might be found downstream of CHOP, we challenged rat PCNs with high molarity thapsigargin to induce cytotoxicity. The effects of thapsigargin and thapsigargin + ISRIB on cytotoxicity are shown in **Fig. 2D**. Using the LDH assay, the main effect of treatment on cytotoxicity (one-way ANOVA; $F(3, 20) = 9.513$, $p = 0.0004$) was significant. Compared to cells treated with vehicle control, cells treated with 10 μM thapsigargin (Bonferroni's MCT, $p = 0.0028$), 10 μM thapsigargin + 200 nM ISRIB (Bonferroni's MCT, $p = 0.0004$), or 10 μM thapsigargin + 1 μM ISRIB (Bonferroni's MCT, $p = 0.0079$) had increased cytotoxicity. No significant differences were observed in cells treated with thapsigargin compared to cells treated with thapsigargin + ISRIB ($p > 0.9999$). These data confirm that thapsigargin is a potent generator of ER stress and that it induces the translation of key modulators of the UPR. Thapsigargin-induced ATF4 translation was mitigated by the addition of ISRIB- further confirming appropriate target engagement. Not surprisingly, ISRIB did not confer neuroprotection against thapsigargin at challenge doses beyond those capable of inducing CHOP. Together, these results indicate that ER stress can be successfully modeled and modulated *in vitro* using thapsigargin and ISRIB in rat PCNs. Furthermore, the results of this experiment were used to guide our *in vitro* studies in the $APP^{Swe}$ model of amyloidosis.

*$APP^{Swe}$ PCNs showed no evidence of ER stress-related dysfunction in vitro despite evidence of ISRIB target engagement*

Because ER stress has been implicated in the pathogenesis of AD, we assessed its involvement and response to thapsigargin *in vitro* using PCNs generated from $APP^{Swe}$ nTg and Tg mice. In addition, beta-site APP-cleaving enzyme 1 (BACE1), the enzyme responsible for increased production of Aβ in $APP^{Swe}$ mice, is one of few exceptions whose mRNA translation is up-regulated by eIF2α phosphorylation (De Pietri Tonelli et al., 2004; Lammich et al., 2004;

Mihailovich et al., 2007; O'Connor et al., 2008; Devi and Ohno, 2010; Scheper and Hoozemans, 2015). To investigate the ER stress pathway and the effects of its modulation, cells were treated with vehicle, 1 μM thapsigargin, or 1 μM thapsigargin + 200 nM ISRIB as guided by our previous experiments. Because thapsigargin successfully induced, and ISRIB successfully mitigated, the induction of ATF4 in rat PCNs, we focused on this marker in $APP^{Swe}$ PCNs and the results are shown in **Fig. 3**. The main effect of treatment on levels of ATF4 (one-way ANOVA; $F(5, 12) = 50.80$, $p < 0.0001$) was significant and is shown in **Fig. 3A**. Compared to nTg cells treated with vehicle control, nTg cells treated with 1 μM thapsigargin (Bonferroni's MCT, $p < 0.0001$) and 1 μM thapsigargin + 200 nM ISRIB (Bonferroni's MCT, $p < 0.0001$) had increased levels of ATF4. Similarly, Tg cells treated with 1 μM thapsigargin (Bonferroni's MCT, $p < 0.0001$) and 1 μM thapsigargin + 200 nM ISRIB (Bonferroni's MCT, $p < 0.0001$) had increased levels of ATF4 compared to cells treated with vehicle. No differences were found between genotypes in levels of ATF4, regardless of treatment. To ensure these outcomes were not the result of inadequate ISRIB target engagement, the experiment was repeated in nTg cells cultured for 7 and 11 DIV. Half of the cells were allocated for analysis using the SUnSET technique (Schmidt et al., 2009) to examine the effects of ISRIB on global protein synthesis. The remaining half were used to examine the effects of ISRIB on thapsigargin-induced ATF4 expression (as described above). The results of the SUnSET experiment in cells cultured for 7 DIV are shown in **Fig. 3B**. Cells treated with thapsigargin + puromycin (M = 0.4275, SD = 0.03957) had reduced levels of puromycinylated protein compared to cells treated with vehicle + puromycin (M = 1.139, SD = 0.1167); $t(7) = 12.93$, $p < 0.0001$. Cells treated with thapsigargin + ISRIB + puromycin (M = 0.7267, SD = 0.1228) had reduced levels of puromycinylated protein compared to cells treated with vehicle + puromycin; $t(7) = 5.115$, $p = 0.0014$. Finally, cells treated with thapsigargin + ISRIB + puromycin (M = 0.7267, SD = 0.1228) had increased levels of puromycinylated protein compared to cells treated with thapsigargin + puromycin (M = 0.4275, SD = 0.03957); $t(8) =$

5.185, $p$ = 0.0008. This experiment was repeated in cells cultured for 11 DIV and similar results were found (data not shown). In this experiment, cells treated with thapsigargin + puromycin and thapsigargin + ISRIB + puromycin had reduced levels of puromycinylated protein compared to cells treated with vehicle + puromycin ($p$ < 0.0001 and $p$ = 0.001, respectively). Again, cells treated with thapsigargin + ISRIB + puromycin had increased levels of puromycinylated protein ($p$ = 0.0013) Compared to cells treated with thapsigargin + puromycin. Having established proof of ISRIB target engagement, as evidenced by restoration of protein synthesis, we next evaluated the levels of ATF4 in response to thapsigargin challenge in cells cultured for 7 DIV and the results are shown in **Fig. 3C**. Cells treated with thapsigargin (M = 0.7311, SD = 0.1841) had increased levels of ATF4 compared to cells treated with vehicle (M = 0.01943, SD = 0.01355); $t$(10) = 9.444, $p$ < 0.0001, as did cells treated with thapsigargin + ISRIB (M = 0.7651, SD = 0.4040); $t$(10) = 4.518, $p$ = 0.0011. This experiment was repeated in cells cultured for 11 DIV (data not shown) and similar results were found. Cells treated with thapsigargin or thapsigargin + ISRIB had increased levels of ATF4 compared to cells treated with vehicle ($p$ < 0.0001 and $p$ = 0.0122, respectively). While cells cultured for 11 DIV treated with thapsigargin + ISRIB had a modest reduction in levels of ATF4 compared to cells treated with thapsigargin-only, the results were not significant ($p$ = 0.137). Together, these results indicate that PCNs cultured from $APP^{Swe}$ mice showed no evidence of ER-stress related dysfunction and, despite restoring thapsigargin-induced translational repression, ISRIB did not mitigate thapsigargin-induced ATF4 expression.

**ISRIB pharmacokinetics and tolerability in C57BL/6J mice *in vivo***

Prior to examining the role of ER stress and its modulation in PS19 and $APP^{Swe}$ mice, we needed to ensure that ISRIB crossed the blood brain barrier (BBB) and that prolonged, once daily dosing could be tolerated. To determine if ISRIB permeated the brain, C57BL/6J mice received a single IP injection of vehicle of ISRIB (5 mg/kg). Brain and plasma were collected at 5 time points following the injection: immediately (data not shown-ISRIB undetectable), 0.5, 2, 4,

and 8 hours. As shown in **Fig. 4A**, ISRIB was successfully detected in brain and plasma at all collection points. ISRIB concentration could not be predicted by time, neither in brain (4.099*h + 108.9, $R^2$ = 0.08998) nor plasma (1.564*h + 157.7, $R^2$ = 0.004507). Secondary analysis by two-way ANOVA confirmed there was no effect of collection time ($F$(3, 23) = 0.6006, $p$ = 0.6212) or collection source ($F$(1, 23) = 3.539, $p$ = 0.0726) on ISRIB concentration. To ensure chronic ISRIB administration did not have any adverse effects on body weight or mortality *in vivo*, C57BL/6J mice received one IP injection per day of vehicle or ISRIB (5 mg/kg) for 9 weeks. The effect of prolonged, once daily ISRIB administration in C57BL/6J mice on body weight is shown in **Fig. 4B**. The main effect of time on body weight ($F$(8, 80) = 20.26, $p$ < 0.0001) was significant; however, the effect of treatment on body weight ($F$(1, 10) = 0.8533, $p$ = 0.3774) was not (1 x 9 SPANOVA). The effect of ISRIB on mortality in C57BL/6J mice is shown in **Fig. 4C**. No difference in the survival distribution was found between mice treated with vehicle and mice treated with ISRIB (Mantel-Cox; $\chi^2$ = 1.000, $p$ = 0.3173). Together, these results confirmed that ISRIB permeated the brain and that chronic, once daily dosing was well tolerated by C57BL/6J mice.

**Tolerability to prolonged ISRIB administration in PS19 mice *in vivo***

To investigate the role of ER stress in the AD-like manifestations observed in PS19 mice, nTg and Tg mice received once daily injections of either vehicle or ISRIB (5 mg/kg) for 9 weeks while undergoing behavioral testing. The effects of prolonged, once daily administration of vehicle or ISRIB on body weight and mortality are shown in **Fig. 5**. The effects of genotype and treatment on body weight are shown in **Fig. 5A**. The main effects of time ($F$(8, 784) = 104.4, $p$ < 0.0001) and group (i.e., genotype & treatment; $F$(3, 98) = 11.42, $p$ < 0.0001) as well as their interaction ($F$(24, 784) = 1.722, $p$ = 0.0173) were significant (6 x 9 SPANOVA). Compared to nTg mice treated with vehicle, nTg mice treated with ISRIB weighed significantly less on weeks 5, 7, 8, and 9 (Bonferroni's MCT, $p$ < 0.05). Compared to nTg mice treated with vehicle, Tg mice treated with

vehicle weighed significantly less for the duration of the study (Bonferroni's MCT; weeks 1 and 3, $p < 0.01$; week 2, 4, and 5, $p < 0.001$; weeks 6 - 9, $p < 0.0001$). Compared to nTg mice treated with vehicle, Tg mice treated with ISRIB weighed significantly less on all but week 1 (Bonferroni's MCT; weeks 2 - 4, $p < 0.01$; week 5, $p < 0.001$; weeks 6 - 9, $p < 0.0001$). The effects of genotype and treatment on survival rate in PS19 mice are shown in **Fig. 5B**. Compared to nTg mice treated with vehicle, nTg mice treated with ISRIB had a significantly higher survival rate (Mantel-Cox; $\chi^2 = 6.535$, $p = 0.0106$). Compared to nTg mice treated with vehicle, Tg mice treated with vehicle (Mantel-Cox; $\chi^2 = 12.91$, $p = 0.0003$) and Tg mice treated with ISRIB (Mantel-Cox; $\chi^2 = 7.841$, $p = 0.0051$) had significantly lower survival rates. There were no differences in the survival distribution of Tg mice treated vehicle and Tg mice treated with ISRIB (Mantel-Cox; $\chi^2 = 0.6417$, $p = 0.4231$). These results confirm that PS19 Tg mice exhibit phenotypically reduced body weight (Lopez-Gonzalez et al., 2015) and increased mortality (Yoshiyama et al., 2007) as previously reported. Based on these outcomes, prolonged, once daily administration of ISRIB was well tolerated by PS19 mice. These data provide assurance that behavioral outcomes, subsequently described, can be attributed to inherent genotype-dependent behavioral deficits and are not likely the result of a negative visceral reaction to the compounds used presently.

**Effects of genotype and eIF2B modulation on behavioral outcomes in PS19 mice *in vivo***

PS19 Tg mice have been reported to exhibit behavioral impairments including deficits in spatial and fear-based learning and memory (Takeuchi et al., 2011; Min et al., 2015; Lasagna-Reeves et al., 2016). To ensure that PS19 Tg mice expressed behavioral impairments consistent with those previously described and to investigate if ER stress was implicated in those deficits, PS19 mice underwent extensive behavioral testing and the results are shown in **Fig. 6**.

*PS19 Tg mice exhibit locomotor hyperactivity*

To assess locomotor activity, mice were tested in the activity chamber at 4 different time points throughout the study and the results are shown in **Fig. 6A-C**. The quantification of ambulatory

595 distance is shown in **Fig. 6A**. The main effects of activity chamber test number (two-way RM
596 ANOVA; $F(3, 294) = 6.455$, $p = 0.0003$) and group (two-way RM ANOVA; $F(3, 98) = 4.056$, $p =$
597 0.0092) were significant. Compared to nTg mice treated with ISRIB, Tg mice treated with ISRIB
598 ambulated a greater distance on test 3 (Bonferroni's MCT, $p < 0.01$). The quantification of
599 ambulatory duration is shown in **Fig. 6B**. The main effects of activity chamber test number (two-
600 way RM ANOVA; $F(3, 294) = 5.847$, $p = 0.0007$) and group (two-way RM ANOVA; $F(3, 98) =$
601 3.658, $p = 0.0151$) were significant. Compared to nTg mice treated with ISRIB, Tg mice treated
602 with ISRIB had longer ambulatory durations on tests 2 and 3 (Bonferroni's MCT, $p < 0.05$). The
603 quantification of rearing frequency is shown in **Fig. 6C**. The main effects of activity chamber test
604 number (two-way RM ANOVA; $F(3, 294) = 9.866$, $p < 0.0001$) and group (two-way RM ANOVA;
605 $F(3, 98) = 5.879$, $p = 0.0010$) were significant. Compared to nTg mice treated with vehicle, Tg
606 mice treated with vehicle reared more frequently on test 2 (Bonferroni's MCT, $p < 0.05$).
607 Compared to nTg mice treated with ISRIB, Tg mice treated with ISRIB reared more frequently on
608 tests 3 (Bonferroni's MCT, $p < 0.01$) and 4 (Bonferroni's MCT, $p < 0.05$). For the sake of
609 analyzing the phenotype, PS19 Tg mice treated vehicle were compared to PS19 nTg mice
610 treated with vehicle. The data from each AC test measure was pooled and analyzed using t-tests
611 (unpaired, two-tailed). Tg mice treated with vehicle ambulated a further distance (M = 2753, SD
612 = 1107) than nTg mice treated with vehicle (M = 2336, SD = 711.5); $t(206) = 3.256$, $p = 0.0013$.
613 Tg mice treated with vehicle spent more time ambulating (M = 93.32, SD = 41.64) than nTg mice
614 treated with vehicle (M = 79.60, SD = 25.69); $t(206) = 2.884$, $p = 0.0043$. Finally, PS19 Tg mice
615 treated with vehicle reared more frequently (M = 132.0, SD = 71.74) than nTg mice treated with
616 vehicle (M = 94.31, SD = 54.25); $t(206) = 4.297$, $p < 0.0001$. These results confirm that PS19 Tg
617 mice express locomotor hyperactivity- consistent with their behavioral phenotype. A summary of
618 all behavioral outcomes used for phenotype analysis in PS19 mice are provided in **Table 3**.

619 *PS19 Tg mice exhibit diminished anxiety-like behavior*

To examine anxiety-like behavior, PS19 mice were tested using the EPM and the results are shown in **Fig. 6D**. The main effect of genotype on time spent in the open arms (one-way ANOVA; $F(3, 93) = 6.977$, $p = 0.0003$) was significant. Compared to nTg mice treated with vehicle, Tg mice treated with vehicle (Bonferroni's MCT, $p < 0.001$) and Tg mice treated with ISRIB (Bonferroni's MCT, $p < 0.01$) spent a larger percentage of time in the open arms than the closed arms. These results confirm that PS19 Tg mice exhibit reduced anxiety-like behavior.

*PS19 Tg mice exhibit spatial learning and memory deficits with modest restoration of spatial acquisition by ISRIB*

To assess spatial learning and memory, mice were tested using the MWM and the results are shown in **Fig. 6E-G**. The main effects of test day ($F(4, 280) = 106.6$, $p < 0.0001$) and group ($F(3, 70) = 13.76$, $p < 0.0001$) on escape latency (i.e., latency to locate and climb atop the platform) were significant (two-way RM ANOVA) as shown in **Fig. 6E**. Compared to nTg mice treated with vehicle, Tg mice treated with vehicle had longer escape latencies on all training days: days 1, 2, and 5 (Bonferroni's MCT, $p < 0.0001$), days 3 and 4 (Bonferroni's MCT, $p < 0.001$). Compared to nTg mice treated with vehicle, Tg mice treated with ISRIB had longer escape latencies on days 1 and 2 (Bonferroni's MCT, $p < 0.01$). Compared to nTg mice treated with ISRIB, Tg mice treated with ISRIB took longer to escape on day 2 (Bonferroni's MCT, $p < 0.01$). Performance in Tg mice treated with ISRIB was restored to near nTg levels on days 3, 4, and 5. To assess learning over time, performance on subsequent training days was compared within groups to performance on day 1. All groups performed significantly better on day 5 compared to day 1 ($p < 0.0001$), indicating that all groups acquired the task. To assess spatial memory recall, a probe test was administered 24 and 72 hours following completion of the acquisition phase of the MWM. The percentage of time spent in the target and nontarget quadrants was assessed using paired-samples t-tests. The effects of genotype and treatment on recall during the 24 hour probe test are shown in **Fig. 6F**. nTg mice treated with vehicle spent more time in the target quadrant (M =

43.3535, SD = 9.751) than the nontarget quadrant (M = 18.9039, SD = 3.252); $t(22) = 9.018$, $p = < 0.0001$, and nTg mice treated with ISRIB spent more time in the target quadrant (M = 41.1725, SD = 13.06) than the nontarget quadrant (M = 19.6304, SD = 4.351); $t(23) = 6.063$, $p = < 0.0001$. No significant differences in quadrant duration were found in Tg mice. The results of the 72 hour probe test are shown in **Fig. 6G**. nTg mice treated with vehicle spent more time in the target quadrant (M = 40.6565, SD = 11.04) than the nontarget quadrant (M = 19.813, SD = 3.691); $t(22) = 6.787$, $p < 0.0001$, and nTg mice treated with ISRIB spent more time in the target quadrant (M = 36.5083, SD = 15.43) than the nontarget quadrant (M = 21.1833, SD = 5.140); $t(23) = 3.650$, $p = 0.0013$. No significant differences in quadrant duration were found in Tg mice. To control for the confounding effect of vision impairments in PS19 mice, a visual platform test was administered 24 hours later (data not shown) and the main effect of group on escape latency was found to be significant (one-way ANOVA; $F(3, 70) = 15.87$, $p < 0.0001$). As such, mice that met the exclusion criteria (as described in the methods) were retrogradely excluded from the study. These results indicate that ISRIB confers partial restoration of spatial learning deficits in Tg mice. By extension, these data suggest that ER stress, abbreviated presently by ISRIB, may be implicated in the behavioral manifestations observed in the PS19 model of tauopathy.

*PS19 Tg mice do not exhibit impairments in fear-based learning and memory*

To investigate fear-based learning and memory, the passive avoidance test was used and the results are shown in **Fig. 6H**. No significant differences were found between groups during the habituation (one-way ANOVA; $F(3, 77) = 0.5574$, $p = 0.6448$), training (one-way ANOVA; $F(3, 78) = 0.5432$, $p = 0.6542$), or recall (one-way ANOVA; $F(3, 78) = 01.292$, $p = 0.2833$) phases of the test. The main effect of task phase was found to be significant $F(2, 234) = 78.50$, $p < 0.0001$. Compared to the training phase, all groups took significantly longer to cross during the testing phase ($p < 0.0001$, Bonferroni's MCT). These results indicate that all mice learned and recalled the test and that Tg mice do not display impaired fear-based learning and memory.

**Effects of genotype and eIF2B modulation on neuropathology in PS19 mice**

PS19 Tg mice develop a robust neuropathology characterized by aberrant accumulations of hyper-phosphorylated tau and neuronal loss (Yoshiyama et al., 2007) and components of the PERK pathway may be implicated in this pathogenesis (Hoozemans et al., 2009; Salminen et al., 2009; Ho et al., 2012) and possibly contribute to behavioral impairments. Because a modest restoration of spatial memory acquisition was observed in Tg mice treated with ISRIB, we were interested to assess levels of ER stress-related markers ex vivo. Upon completion of behavioral testing, PS19 mice were sacrificed and their brains assessed for levels of ATF4, CHOP, and the development of AD-like neuropathology. The results of these analyses are shown in **Fig. 7** and **Fig. 8**. Immunoblots of cortical tissue homogenates were probed for ATF4, CHOP, and tubulin (internal loading control) as shown in **Fig. 7A**. Lysate from E17 rat PCNs treated with thapsigargin was used as a positive control (+ control). CHOP was undetectable in PS19 mice (see **Fig. 7A**) and no significant differences in levels of ATF4 were found (one-way ANOVA; $F(3, 37) = 1.018$, $p = 0.3958$) as shown in **Fig. 7B**. Immunoblots of hippocampal homogenates were probed for p-tau (AT8), total tau (Tau5), and GAPDH (internal loading control) as shown in **Fig. 7C**. Student's t-test revealed that Tg mice treated with ISRIB had more p-tau in the hippocampus (M = 0.8933, SD = 0.5938) than Tg mice treated with vehicle (M = 3.406, SD = 2.201); $t(12) = 2.699$, $p = 0.0193$ as shown in **Fig. 7D**. No difference was found in levels of Tau5 (M = 1.957, SD = 1.109) or GAPDH (M = 1.874, SD = 0.9811); $t(13) = 0.1546$, $p = 0.8795$ as shown in **Fig. 7D.** To determine if the development of tau pathology was region-specific, immunohistochemistry (IHC) was performed and the regions of interest (ROIs) are indicated in **Fig. 8A** along with 2.5x photomicrographs of the hippocampus in nTg and Tg mice, treated with and without ISRIB. Representative photomicrographs (40x) of the dentate gyrus (DG) are shown in **Fig. 8B**. A main effect of group on the number of p-tau positive inclusions in the DG (one-way ANOVA; $F(3, 24) = 6.165$, $p = 0.0029$) was found to be significant and the results are shown in **Fig. 8C**. Compared

to nTg mice treated with vehicle, Tg mice treated with ISRIB (Bonferroni's MCT, $p < 0.05$) had significantly more p-tau in the DG. A significant main effect of group was also found on levels of p-tau in CA1 of the hippocampus (data not shown; one-way ANOVA; $F(3, 24) = 3.213$, $p = 0.0408$). While the results were not significant, Tg mice also had more p-tau in CA3 compared to nTg mice treated with vehicle (data not shown; one-way ANOVA; $F(3, 24) = 2.723$, $p = 0.0667$). The total number of p-tau positive inclusions summed across all regions of the hippocampus was found to be significant and the results are shown in **Fig. 8D** (one-way ANOVA; $F(3, 80) = 9.547$, $p < 0.0001$). Compared to nTg mice treated with vehicle, Tg mice treated with vehicle or ISRIB had increased levels of p-tau (Bonferroni's MCT, $p < 0.01$) throughout the hippocampus. In addition, evidence of neuronal loss and hippocampal atrophy was observed in Tg mice. Representative photomicrographs (2.5x) of the hippocampus stained with fluoro-nissl are shown in **Fig. 8E**. Arrows indicate the pyramidal cell layer of CA1. The main effect of group on CA1 pyramidal cell layer thickness was found to be significant (one-way ANOVA; $F(3, 164) = 11.28$, $p < 0.0001$) and the results are shown in **Fig. 8F**. Compared to nTg mice treated with vehicle, Tg mice treated with vehicle or ISRIB had significant thinning of the CA1 pyramidal cell layer (Bonferroni's MCT, $p < 0.01$) to indicate neuronal loss. Together, these results confirm that PS19 Tg mice develop a significant neuropathology to include increased p-tau, and hippocampal atrophy indicative of neuronal loss. Interestingly, PS19 mice showed no evidence of ER stress-related increases in ATF4 or CHOP. Paradoxically, Tg mice treated with ISRIB, despite improved spatial memory acquisition, developed a worsened p-tau neuropathology. While no evidence of ER stress was found in this study, these data suggest that antagonism of eIF2B using ISRIB may restore translational repression in the PS19 mouse model of AD leading to an increased in tau phosphorylation.

**Tolerability of APP$^{Swe}$ mice to ISRIB administration *in vivo***

Next, we investigated the role of ER stress and eIF2B modulation on the AD-like manifestations observed in the $APP^{Swe}$ mouse model of AD. The effects of genotype and treatment on body weight and survival in $APP^{Swe}$ mice are shown in **Fig. 9**. The same dosing paradigm used for C57BL/6J and PS19 mice- once daily administration of vehicle or ISRIB (5 mg/kg)- resulted in significant mortality in $APP^{Swe}$ mice by the 8th day of treatment. As such, the protocol was modified and mice received daily injections of vehicle or ISRIB (0.25 or 2.5 mg/kg) only on behavioral test days. The effects of treatment on body weight in nTg and Tg mice are shown in **Fig. 9A**. The main effects of week ($F(11, 594) = 18.84$, $p < 0.0001$) and group ($F(3, 54) = 3.896$, $p = 0.0136$) as well as their interaction ($F(33, 594) = 1.544$, $p = 0.0284$) were significant (6 x 12 SPANOVA). Compared to nTg mice treated with vehicle, Tg mice treated with vehicle weighed less on weeks 1, 7, 10, and 11 (Bonferroni's MCT, $p < 0.05$). Compared to nTg mice treated with vehicle, Tg mice treated with ISRIB weighed less on weeks 7 and 11 (Bonferroni's MCT, $p < 0.05$). The effects of genotype and treatment on mortality rate are shown in **Fig. 9B**. Compared to nTg mice treated with vehicle, nTg mice treated with ISRIB had a lower survival rate (Mantel-Cox; $\chi^2 = 6.846$, $p = 0.0089$). Compared to nTg mice treated with vehicle, Tg mice treated with vehicle (Mantel-Cox; $\chi^2 = 6.480$, $p = 0.0109$) had a lower survival rate. Finally, compared to Tg mice treated with vehicle, Tg mice treated with ISRIB had a lower survival rate (Mantel-Cox; $\chi^2 = 6.923$, $p = 0.0085$). Together, these data indicate that $APP^{Swe}$ Tg mice have slightly lower body weights compared to nTg mice and that modulation of components in the PERK-eIF2α pathway may have adverse effects in this mouse model of amyloidosis.

**Effects of genotype and eIF2B modulation on behavioral outcomes in $APP^{Swe}$ mice *in vivo***

$APP^{Swe}$ Tg mice have been found to express an AD-like age-dependent phenotype characterized by learning and memory impairment (Hsiao et al., 1996). To ensure that $APP^{Swe}$ Tg mice expressed behavioral impairments consistent with those previously reported and to investigate if eIF2B modulation using ISRIB could restore these deficits, $APP^{Swe}$ mice underwent extensive

behavioral testing and the results are shown in **Fig. 10**. A summary of all behavioral outcomes analyzed for phenotype in $APP^{Swe}$ mice are provided in **Table 4**.

*$APP^{Swe}$ Tg mice exhibit locomotor hyperactivity*

To determine the effects of genotype and treatment on locomotor activity, $APP^{Swe}$ mice were tested in the activity chamber and the results are shown in **Fig. 10A, B**. A main effect of group on ambulatory distance (one-way ANOVA; $F(3, 51) = 3.794$, $p = 0.0157$) was found to be significant as shown in **Fig. 10A**. Compared to nTg mice treated with ISRIB, Tg mice treated with ISRIB moved a greater distance (Bonferroni's MCT, $p = 0.0140$). A main effect of group on center duration (one-way ANOVA; $F(3, 53) = 8.377$, $p = 0.0001$) was found to be significant as shown in **Fig. 10B**. Compared to nTg mice treated with vehicle, Tg mice treated with vehicle (Bonferroni's MCT, $p = 0.0019$) or ISRIB (Bonferroni's MCT, $p = 0.0239$) spent more time in the center of the activity chamber.

*$APP^{Swe}$ Tg mice exhibit deficits in fear-based learning and memory*

To assess the effects of genotype and treatment on fear-associated learning and memory, $APP^{Swe}$ mice underwent fear conditioning followed by cued- or context-based retrieval testing. The results are shown in **Fig. 10C**, **D**. For fear conditioning, the main effects of trial ($F(4, 216) = 50.36$, $p < 0.0001$) and group ($F(3, 54) = 8.473$, $p = 0.0001$) as well as their interaction ($F(12, 216) = 5.070$, $p < 0.0001$) were significant (6 x 5 SPANOVA) as shown in **Fig. 10C**. Compared to nTg mice treated with vehicle, Tg mice treated with vehicle or ISRIB (Bonferroni's MCT, $p < 0.0001$) froze less during ITI2. Compared to nTg mice treated with ISRIB, Tg mice treated with ISRIB froze less during tone 2 (Bonferroni's MCT, $p < 0.01$) and ITI2 (Bonferroni's MCT, $p < 0.0001$). The main effect of group on context-based retrieval (one-way ANOVA; $F(3, 54) = 9.530$, $p < 0.0001$) was significant as shown in **Fig. 10D**. Compared to nTg mice treated with vehicle, Tg mice treated with vehicle (Bonferroni's MCT, $p = 0.0079$) or ISRIB (Bonferroni's MCT, $p =$

0.0008) froze less and while the results were not significant ($p$ = 0.0662), Tg mice also froze less than nTg mice during cue-based retrieval.

*$APP^{Swe}$ Tg mice do not exhibit impairments in spatial learning and memory*

To assess the effects of genotype and treatment on spatial learning and memory, $APP^{Swe}$ mice were tested using the MWM and the results are shown in **Fig. 10E, F**. The main effect of test day ($F$(4, 480) = 5.602, $p$ = 0.0002) on escape latency was found to be significant (4 x 4 SPANOVA) as shown in **Fig. 10E**. Compared to day 1, nTg mice treated with vehicle located the platform faster on day 5 (Bonferroni's MCT, $p$ = 0.0017). Compared to day 1, Tg mice treated with vehicle located the platform faster on days 3 (Bonferroni's MCT, $p$ = 0.0111), 4 (Bonferroni's MCT, $p$ = 0.0416), and 5 (Bonferroni's MCT, $p$ = 0.0026). No significant between-group differences were found on any of the test days ($p$ = 0.0891). To ensure that mice had acquired the task, a reversal trial was conducted (see **Fig. 10E** inset) during which the location of the platform was moved. The effect of the reversal trial ($F$(1, 120) = 97.29, $p$ < 0.0001) on escape latency was found to be significant (1 x 4 SPANOVA). Compared to day 5, all groups except nTg mice treated with ISRIB took longer to locate the platform on the reversal trial (Bonferroni's MCT, $p$ < 0.0001). During the probe test to assess spatial memory recall, percentage time spent in the target and nontarget quadrants was analyzed using paired-samples t-tests and the results are shown in **Fig. 10F**. nTg mice treated with vehicle spent more time in the target quadrant (M = 35.25, SD = 10.97) than the nontarget quadrant (M = 21.60, SD = 3.658); $t$(9) = 2.950, $p$ = 0.0162 as did nTg mice treated with ISRIB (target: M = 45.86, SD = 10.76, nontarget: M = 18.062, SD = 3.586; $t$(3) = 3.876, $p$ = 0.0304), Tg mice treated with vehicle (target: M = 38.56, SD = 14.23, nontarget: M = 20.50, SD = 4.744; $t$(10) = 3.157, $p$ = 0.0102), and Tg mice treated with ISRIB (target: M = 39.07, SD = 11.36, nontarget: M = 20.33, SD = 3.786; $t$(5) = 3.031, $p$ = 0.0290).

*$APP^{Swe}$ Tg mice exhibit deficits in spatial working and recognition memory*

To assess the effects of genotype and treatment on spatial working memory, the Y-maze was used and the results are shown in **Fig. 10G**. nTg mice treated with vehicle had a significantly greater percent alternation compared to 50% chance alternation (M = 62.17, SD = 6.181); $t(12) = 7.099$, $p < 0.0001$. No significant differences were found between groups in total number of entries or percentage of correct entries in the Y-maze (data not shown). The effects of genotype and treatment on recognition memory were assessed using the NOR test and the results are shown in **Fig. 10H**. Mice were also tested in the NOL test (data not shown); however, all groups failed to show learning. The percentage of time mice spent investigating the novel and non-novel objects was analyzed using paired-samples t-tests. nTg mice treated with vehicle spent more time investigating the novel object (M = 56.24, SD = 24.80) compared to the familiar object (M = 27.85, SD = 13.56); $t(11) = 2.712$, $p = 0.0202$. No significant differences were found between time spent with the novel versus familiar object in nTg mice treated with ISRIB ($p = 0.9224$), Tg mice treated with vehicle ($p = 0.4998$), or Tg mice treated with ISRIB ($p = 0.5838$).

Collectively, $APP^{Swe}$ Tg mice exhibit locomotor hyperactivity, fear-based learning and memory deficits, impaired spatial working memory, and impaired recognition memory. Administration of ISRIB failed to restore any of these learning and memory deficits, indicating that ER stress-related dysfunction, and specifically the downstream effects of PERK-mediated eIF2 phosphorylation, may not mediate the manifestation of the behavioral deficits observed in the $APP^{Swe}$ mouse model of AD.

## DISCUSSION

Emerging evidence suggests that ER stress, and specifically changes in neuronal UPR, may be implicated in the pathogenesis of AD (Paschen and Mengesdorf, 2005a, b; Lindholm et al., 2006; Hoozemans et al., 2009; Scheper and Hoozemans, 2009). ATF4, an integral component of the UPR (Ron and Harding, 2012), is activated by ER stress and regulates the expression of the pro-apoptotic transcription factor CHOP (Ron and Habener, 1992; Averous et al., 2004). The present study aimed to investigate the involvement of ER stress in AD-like outcomes *in vitro*, as measured by ATF4 and CHOP, and *in vivo* using experimental AD models of tauopathy (MAPT P301S) and excessive amyloidosis ($APP^{Swe}$). In addition, the present study investigated if pharmacological modulation of eIF2B signaling cascade, via antagonism of the ISR, could ameliorate AD-like outcomes and implicate ER stress-related dysfunction in the disease pathogenesis of these models.

We hypothesized that ER stress would be involved in the AD-like pathology observed in these models and that ISRIB would mitigate the induction of ATF4 and CHOP *in vitro* and *in vivo*. We also hypothesized that ER stress-related dysfunction may contribute to the AD-like behavioral impairments observed in PS19 and $APP^{Swe}$ Tg mice. Furthermore, we predicted that ISRIB would restore inherent deficits in learning and memory *in vivo* and curtail the underlying neuropathology responsible for these behavioral deficits.

In this study, we found that thapsigargin effectively induced ATF4, CHOP, and at higher concentrations, cytotoxicity, in PCNs derived from rats. Recently, ISRIB was found to mitigate the induction of ATF4 and CHOP in response to ER stress in HEK293 and U2OS cells (Sidrauski et al., 2013). We were able to partially corroborate those findings in rat PCNs. Despite a significant reduction in ATF4, ISRIB did not fully antagonize the effects of thapsigargin (i.e., CHOP) under the conditions used. Since ISRIB successfully mitigated the induction of ATF4 to indicate appropriate target engagement, we focused on ATF4 as a marker of ER stress.

As was observed in rat PCNs, thapsigargin also induced ATF4 in PCNs derived from $APP^{Swe}$ nTg and Tg mice. Interestingly, basal levels of ATF4 were undetectable in both $APP^{Swe}$ nTg and Tg cells, indicating that Tg cells show no evidence of constitutive ATF4 translation to indicate ER stress-related dysfunction. This was surprising since previously it was reported that eIF2α phosphorylation can occur in response to Aβ in cultured cells expressing Swe-APP (Kim et al., 2007). As such, it is possible that the Tg PCNs used in the present study had yet to express the Aβ pathology required to compromise PERK-eIF2α signaling and increase ER stress-related markers. We also found that thapsigargin induced comparable levels of ATF4 in nTg and Tg $APP^{Swe}$ PCNs, indicating that cells isolated from Tg mice respond appropriately to ER stress. Presently, we were unable to mitigate the effects of thapsigargin on ATF4 induction using ISRIB in $APP^{Swe}$ PCNs. While ISRIB seemed to capable of reversing the translational inhibition induced by thapsigargin, this outcome appears to be independent of the ATF4 cascade. Under the same conditions, ISRIB reduced thapsigargin-induced ATF4 in rat PCNs cultured for 12–13 DIV. Because we observed a non-significant trend toward reduced ATF4 in mouse PCNs cultured for 11 DIV (data not shown), it is possible that a more pronounced reduction would be observed in cells cultured for longer periods of time or challenged with a reduced concentration of thapsigargin. Another possible explanation is that thapsigargin induces ATF4 through mechanisms other than deactivation of eIF2B. Despite our knowledge that ER stress can trigger the activation of ATF4, the functional role of ATF4 in the ER stress response is still not fully understood (Galehdar et al., 2010). Therefore, it is possible that downstream effects of the UPR and ISR can occur in the absence of ATF4 activity. In line with this possibility, a recent study found that deletion of ATF4 in liver was not required for the induction of the UPR transcription factor CHOP, but rather, ATF6 was found to be the primary inducer of CHOP (Fusakio et al., 2016).

Recently, the therapeutic effects of PERK modulation using ISRIB have been assessed using *in vivo* models of neurodegeneration (Halliday et al., 2015; Johnson and Kang, 2016). To investigate the role of ER stress and the effects of PERK pathway modulation in PS19 and $APP^{Swe}$ *in vivo*, mice underwent extensive behavioral testing. In line with previous reports, PS19 Tg mice had reduced body weight, increased mortality and expressed a behavioral phenotype characterized by locomotor hyperactivity, diminished anxiety-like behavior (Lopez-Gonzalez et al., 2015), and behavioral impairment (Takeuchi et al., 2011; Min et al., 2015). Aside from a modest improvement in spatial memory acquisition in the MWM, pharmacological antagonism of the ISR using ISRIB was minimally effective at restoring the behavioral deficits observed in PS19 Tg mice. However, postmortem analysis revealed no evidence of ER stress-related induction in PS19 Tg mice, who had comparable levels of ATF4 in the hippocampus to nTg mice. This may again indicate a lack of target presence or activation, and therefore engagement, upstream of ATF4. For example, in prion-diseased mice with elevated ISR activity, ISRIB was found to exert therapeutic effects (Halliday et al., 2015). In this model, ISRIB prevented neuronal loss in the hippocampus, reduced levels of ATF4, and prevented the development of prion spongiform pathology. ISRIB also slowed the progression of prion disease by preventing the development of confirmatory signs including deficits in balance and motor coordination and sensorimotor impairment (Halliday et al., 2015). Another possibility is that the mechanisms that govern ER stress related pathways and the development of AD-like neuropathologies are not conserved across animal models of AD or their *in vitro* counterparts. For example, while elevated levels of ATF4 have been reported in the hippocampus of APP-PS1 (Ma et al., 2013), 5xFAD (Devi and Ohno, 2013), and APOE4 mice (Segev et al., 2015), ATF4 was not detected in neither the cortex nor hippocampus of hAPP-J20 mice (Johnson and Kang, 2016).

Despite lack of evidence for ER stress-related dysfunction, PS19 Tg mice developed significant hippocampal atrophy evidenced by reductions in the pyramidal cell layer of CA1.

885 Similarly, in human AD, ~70% of neurons in CA1 of the hippocampus have been found to die
886 during the progression of the disease (West et al., 1994). Previous studies employing the PS19
887 model have reported signs of synaptic dysfunction in CA1/CA3 (Yoshiyama et al., 2007),
888 neuronal apoptosis in CA1, CA3, and the DG (Lopez-Gonzalez et al., 2015), and hippocampal
889 atrophy (Min et al., 2015). In line with these previous reports, PS19 Tg mice also developed
890 significant tau pathology. Paradoxically, and despite a slight improvement during the acquisition
891 phase of the MWM, PS19 Tg mice treated with ISRIB had increased p-tau in the DG compared
892 to Tg mice treated with vehicle. These data may suggest that reversal of eIF2α-
893 mediated translational repression by ISRIB may lead to restoration of protein synthesis and as a
894 consequence, an excessive hyper-phosphorylation of tau. Because ISRIB was previously found
895 to improve behavioral function in healthy, WT mice, it is also possible that ISRIB exerts nootropic
896 effects on other pathways to compensate for increased disease pathology. Another possibility is
897 that modulation of the PERK pathway can affect behavioral function through targets other than
898 those implicated in disease pathogenesis. For example, a recent study found that activation of
899 mGluRs, through phosphorylation of eIF2α, induced long-term depression (LTD) by
900 downregulating surface AMPAR density at synapses (Di Prisco et al., 2014) in the hippocampus.
901 Furthermore, hippocampal LTD was found to be crucial for spatial learning of object-place
902 recognition and spatial recognition of objects triggered LTD at Schaffer collateral–CA1 synapses
903 in freely moving animals (Di Prisco et al., 2014). Similarly, increased LTD has been reported in
904 the presence of Aβ oligomers in rat hippocampal slices (Shankar et al., 2008) and several animal
905 models of AD have reported synaptic loss in region proximal to Aβ plaques (Pozueta et al.,
906 2013). Collectively, the loss of functional synapses may underlie the development of learning
907 and memory deficits and behavioral impairments observed in human and animal models of AD
908 (Luscher and Huber, 2010). As such, the identification of additional markers of target

engagement in Tg models of AD, particularly behavioral-related markers, would aid our understanding of disease pathogenesis and its effect on p-eIF2α-dependent LTD.

PS19 mice showed no adverse effects of prolonged, once daily ISRIB administration, yet a significant increase in mortality was observed in $APP^{Swe}$ mice. This may be attributable to some yet unidentified off-target pharmacology. Other studies have reported significant reductions in body weight following long-term ISRIB administration (Halliday et al., 2015) indicating ISRIB may have some level of toxicity. *In vivo*, $APP^{Swe}$ Tg mice displayed behavioral impairments including locomotor hyperactivity and learning and memory deficits (Hsiao et al., 1996; Jacobsen et al., 2006). We observed no therapeutic effect of ISRIB on these behavioral outcomes. However, previous research found no evidence of UPR activation or the induction of cell death pathways in $APP^{Swe}$ mice (Lee et al., 2010b). In addition, a recent study found that ISRIB did not improve deficits in spatial learning and memory In hAPP-J20 Tg mice, nor did it enhance behavioral function in nTg mice (Johnson and Kang, 2016). Based on this research, and our lack of behavioral or *in vitro* evidence to support ER stress-related dysfunction in the disease pathogenesis of $APP^{Swe}$ mice, we did not investigate further those outcomes postmortem.

While ISRIB was minimally effective at improving the learning and memory performance and neuropathological outcomes in these mouse strains, several other compounds targeting the PERK-eIF2$\alpha$ pathway have been found to ameliorate dementia-like or ER-stress related outcomes (Boyce et al., 2005; Kim et al., 2008b; Lee et al., 2010a; Radford et al., 2015). In transgenic mice overexpressing the PS01L mutation, dysregulation of the PERK signaling pathway was associated with the onset of neurodegeneration (Radford et al., 2015). Treatment using a PERK inhibitor (GSK2606414) was reported to prevent further neuronal loss and reduced levels of phosphorylated tau (Radford et al., 2015). However, these mice also had elevated levels of ATF4, and phosphorylated PERK and eIF2$\alpha$ (Radford et al., 2015), providing a platform conducive for target engagement. However, in prion-diseased mice, treatment with

GSK2606414 resulted in significant pancreatic toxicity (Moreno et al., 2013). Salubrinal, a drug that blocks the dephosphorylation of p-eIF2α, has been reported to enhance cell survival *in vitro* following ER stress (Boyce et al., 2005; Kim et al., 2008a). Another study found that treatment with Aβ triggered the UPR in SK-N-SH human neuroblastoma cells, and selective activation of the PERK pathway using Salubrinal prevented Aβ-induced toxicity (Lee et al., 2010a). Collectively, these data suggest that the therapeutic outcomes of PERK-eIF2α pathway modulation are highly dependent on the component targeted in the pathway as well as the disease model in which it is assessed. Because ISRIB targets components downstream of p-eIF2α, this allows for the possibility that further upstream targets may be implicated in the disease pathogenesis of the models used presently.

Taken together, we have shown that modulation of eIF2B mitigated the induction of ATF4 in response to thapsigargin in PCNs derived from rats but not $APP^{Swe}$ mice. While ISRIB exerted minimal therapeutic effects on the neuropathological and behavioral hallmarks observed in PS19 and $APP^{Swe}$ mice, it is important to note that idiosyncrasies in ER stress-related markers were not observed. While it is possible that the therapeutic targets of ISRIB are not implicated or conserved in the AD-like pathology in the animal models examined in this study, these findings warrant further investigation. Future studies might examine the extent to which animal models recapitulate the mechanisms that give rise to AD-like neuropathology and its behavioral correlates. In conclusion, understanding the functional role of ER stress in the pathogenesis of AD is a promising avenue toward the development of more targeted pharmaceuticals. The use of pharmacological tools, such as ISR antagonists, may expedite our understanding of this insidious disease.

## REFERENCES


Alzheimer's A (2013) 2013 Alzheimer's disease facts and figures. Alzheimers Dement 9:208-245.

Ameri K, Harris AL (2008) Activating transcription factor 4. Int J Biochem Cell Biol 40:14-21.

Averous J, Bruhat A, Jousse C, Carraro V, Thiel G, Fafournoux P (2004) Induction of CHOP expression by amino acid limitation requires both ATF4 expression and ATF2 phosphorylation. J Biol Chem 279:5288-5297.

Boyce M, Bryant KF, Jousse C, Long K, Harding HP, Scheuner D, Kaufman RJ, Ma D, Coen DM, Ron D, Yuan J (2005) A selective inhibitor of eIF2alpha dephosphorylation protects cells from ER stress. Science 307:935-939.

De Pietri Tonelli D, Mihailovich M, Di Cesare A, Codazzi F, Grohovaz F, Zacchetti D (2004) Translational regulation of BACE-1 expression in neuronal and non-neuronal cells. Nucleic Acids Res 32:1808-1817.

Devi L, Ohno M (2010) Phospho-eIF2 alpha Level Is Important for Determining Abilities of BACE1 Reduction to Rescue Cholinergic Neurodegeneration and Memory Defects in 5XFAD Mice. Plos One 5.

Devi L, Ohno M (2013) Deletion of the eIF2alpha Kinase GCN2 fails to rescue the memory decline associated with Alzheimer's disease. Plos One 8:e77335.

Di Prisco GV, Huang W, Buffington SA, Hsu CC, Bonnen PE, Placzek AN, Sidrauski C, Krnjevic K, Kaufman RJ, Walter P, Costa-Mattioli M (2014) Translational control of mGluR-dependent long-term depression and object-place learning by eIF2alpha. Nat Neurosci 17:1073-1082.

Fusakio ME, Willy JA, Wang Y, Mirek ET, Al Baghdadi RJ, Adams CM, Anthony TG, Wek RC (2016) Transcription factor ATF4 directs basal and stress-induced gene expression in the unfolded protein response and cholesterol metabolism in the liver. Mol Biol Cell 27:1536-1551.

981 Galehdar Z, Swan P, Fuerth B, Callaghan SM, Park DS, Cregan SP (2010) Neuronal apoptosis
982 induced by endoplasmic reticulum stress is regulated by ATF4-CHOP-mediated induction
983 of the Bcl-2 homology 3-only member PUMA. J Neurosci 30:16938-16948.
984 Gauthier S, Feldman HH, Schneider LS, Wilcock GK, Frisoni GB, Hardlund JH, Moebius HJ,
985 Bentham P, Kook KA, Wischik DJ, Schelter BO, Davis CS, Staff RT, Bracoud L, Shamsi
986 K, Storey JM, Harrington CR, Wischik CM (2016) Efficacy and safety of tau-aggregation
987 inhibitor therapy in patients with mild or moderate Alzheimer's disease: a randomised,
988 controlled, double-blind, parallel-arm, phase 3 trial. Lancet.
989 Halliday M, Radford H, Sekine Y, Moreno J, Verity N, le Quesne J, Ortori CA, Barrett DA,
990 Fromont C, Fischer PM, Harding HP, Ron D, Mallucci GR (2015) Partial restoration of
991 protein synthesis rates by the small molecule ISRIB prevents neurodegeneration without
992 pancreatic toxicity. Cell Death Dis 6.
993 Harding HP, Zhang Y, Ron D (1999) Protein translation and folding are coupled by an
994 endoplasmic-reticulum-resident kinase. Nature 397:271-274.
995 Harding HP, Zhang Y, Bertolotti A, Zeng H, Ron D (2000) Perk is essential for translational
996 regulation and cell survival during the unfolded protein response. Mol Cell 5:897-904.
997 Ho YS, Yang XF, Lau JCF, Hung CHL, Wuwongse S, Zhang QS, Wang JZ, Baum L, So KF,
998 Chang RCC (2012) Endoplasmic Reticulum Stress Induces Tau Pathology and Forms a
999 Vicious Cycle: Implication in Alzheimer's Disease Pathogenesis. J Alzheimers Dis 28:839-
1000 854.
1001 Hoozemans JJ, Veerhuis R, Van Haastert ES, Rozemuller JM, Baas F, Eikelenboom P, Scheper
1002 W (2005) The unfolded protein response is activated in Alzheimer's disease. Acta
1003 Neuropathol 110:165-172.

1004 Hoozemans JJM, van Haastert ES, Nijholt DAT, Rozemuller AJM, Eikelenboom P, Scheper W
1005 (2009) The Unfolded Protein Response Is Activated in Pretangle Neurons in Alzheimer's
1006 Disease Hippocampus. Am J Pathol 174:1241-1251.
1007 Hsiao K, Chapman P, Nilsen S, Eckman C, Harigaya Y, Younkin S, Yang F, Cole G (1996)
1008 Correlative memory deficits, Abeta elevation, and amyloid plaques in transgenic mice.
1009 Science 274:99-102.
1010 Iqbal K, Flory M, Khatoon S, Soininen H, Pirttila T, Lehtovirta M, Alafuzoff I, Blennow K,
1011 Andreasen N, Vanmechelen E, Grundke-Iqbal I (2005) Subgroups of Alzheimer's disease
1012 based on cerebrospinal fluid molecular markers. Ann Neurol 58:748-757.
1013 Jacobsen JS, Wu CC, Redwine JM, Comery TA, Arias R, Bowlby M, Martone R, Morrison JH,
1014 Pangalos MN, Reinhart PH, Bloom FE (2006) Early-onset behavioral and synaptic deficits
1015 in a mouse model of Alzheimer's disease. Proc Natl Acad Sci U S A 103:5161-5166.
1016 Johnson EC, Kang J (2016) A small molecule targeting protein translation does not rescue
1017 spatial learning and memory deficits in the hAPP-J20 mouse model of Alzheimer's
1018 disease. PeerJ 4:e2565.
1019 Kim HS, Choi Y, Shin KY, Joo Y, Lee YK, Jung SY, Suh YH, Kim JH (2007) Swedish amyloid
1020 precursor protein mutation increases phosphorylation of eIF2alpha in vitro and in vivo. J
1021 Neurosci Res 85:1528-1537.
1022 Kim I, Xu W, Reed JC (2008a) Cell death and endoplasmic reticulum stress: disease relevance
1023 and therapeutic opportunities. Nat Rev Drug Discov 7:1013-1030.
1024 Kim I, Xu WJ, Reed JC (2008b) Cell death and endoplasmic reticulum stress: disease relevance
1025 and therapeutic opportunities. Nat Rev Drug Discov 7:1013-1030.
1026 Lammich S, Schobel S, Zimmer AK, Lichtenthaler SF, Haass C (2004) Expression of the
1027 Alzheimer protease BACE1 is suppressed via its 5 '-untranslated region. Embo Rep
1028 5:620-625.

1029 Lasagna-Reeves CA, de Haro M, Hao S, Park J, Rousseaux MW, Al-Ramahi I, Jafar-Nejad P,
1030 Vilanova-Velez L, See L, De Maio A, Nitschke L, Wu Z, Troncoso JC, Westbrook TF,
1031 Tang J, Botas J, Zoghbi HY (2016) Reduction of Nuak1 Decreases Tau and Reverses
1032 Phenotypes in a Tauopathy Mouse Model. Neuron 92:407-418.
1033 Lee DY, Lee KS, Lee HJ, Kim DH, Noh YH, Yu K, Jung HY, Lee SH, Lee JY, Youn YC, Jeong Y,
1034 Kim DK, Lee WB, Kim SS (2010a) Activation of PERK signaling attenuates Abeta-
1035 mediated ER stress. Plos One 5:e10489.
1036 Lee JH, Won SM, Suh J, Son SJ, Moon GJ, Park UJ, Gwag BJ (2010b) Induction of the unfolded
1037 protein response and cell death pathway in Alzheimer's disease, but not in aged Tg2576
1038 mice. Exp Mol Med 42:386-394.
1039 Lenna S, Trojanowska M (2012) The role of endoplasmic reticulum stress and the unfolded
1040 protein response in fibrosis. Curr Opin Rheumatol 24:663-668.
1041 Li J, Ni M, Lee B, Barron E, Hinton DR, Lee AS (2008) The unfolded protein response regulator
1042 GRP78/BiP is required for endoplasmic reticulum integrity and stress-induced autophagy
1043 in mammalian cells. Cell Death Differ 15:1460-1471.
1044 Lindholm D, Wootz H, Korhonen L (2006) ER stress and neurodegenerative diseases. Cell
1045 Death Differ 13:385-392.
1046 Lopez-Gonzalez I, Aso E, Carmona M, Armand-Ugon M, Blanco R, Naudi A, Cabre R, Portero-
1047 Otin M, Pamplona R, Ferrer I (2015) Neuroinflammatory Gene Regulation, Mitochondrial
1048 Function, Oxidative Stress, and Brain Lipid Modifications With Disease Progression in Tau
1049 P301S Transgenic Mice as a Model of Frontotemporal Lobar Degeneration-Tau. J
1050 Neuropathol Exp Neurol 74:975-999.
1051 Luscher C, Huber KM (2010) Group 1 mGluR-dependent synaptic long-term depression:
1052 mechanisms and implications for circuitry and disease. Neuron 65:445-459.

1053 Ma T, Trinh MA, Wexler AJ, Bourbon C, Gatti E, Pierre P, Cavener DR, Klann E (2013)
1054 Suppression of eIF2 alpha kinases alleviates Alzheimer's disease-related plasticity and
1055 memory deficits. Nat Neurosci 16:1299-U1185.
1056 Marciniak SJ, Garcia-Bonilla L, Hu J, Harding HP, Ron D (2006) Activation-dependent substrate
1057 recruitment by the eukaryotic translation initiation factor 2 kinase PERK. J Cell Biol
1058 172:201-209.
1059 Marciniak SJ, Yun CY, Oyadomari S, Novoa I, Zhang Y, Jungreis R, Nagata K, Harding HP, Ron
1060 D (2004) CHOP induces death by promoting protein synthesis and oxidation in the
1061 stressed endoplasmic reticulum. Genes Dev 18:3066-3077.
1062 Mihailovich M, Thermann R, Grohovaz F, Hentze MW, Zacchetti D (2007) Complex translational
1063 regulation of BACE1 involves upstream AUGs and stimulatory elements within the 5 '
1064 untranslated region. Nucleic Acids Research 35:2975-2985.
1065 Min SW et al. (2015) Critical role of acetylation in tau-mediated neurodegeneration and cognitive
1066 deficits. Nat Med 21:1154-1162.
1067 Moreno JA, Halliday M, Molloy C, Radford H, Verity N, Axten JM, Ortori CA, Willis AE, Fischer
1068 PM, Barrett DA, Mallucci GR (2013) Oral treatment targeting the unfolded protein
1069 response prevents neurodegeneration and clinical disease in prion-infected mice. Sci
1070 Transl Med 5:206ra138.
1071 Mullane K, Williams M (2013) Alzheimer's therapeutics: continued clinical failures question the
1072 validity of the amyloid hypothesis-but what lies beyond? Biochem Pharmacol 85:289-305.
1073 O'Connor T, Sadleir KR, Maus E, Velliquette RA, Zhao J, Cole SL, Eimer WA, Hitt B, Bembinster
1074 LA, Lammich S, Lichtenthaler SF, Hebert SS, De Strooper B, Haass C, Bennett DA,
1075 Vassar R (2008) Phosphorylation of the translation initiation factor eIF2alpha increases
1076 BACE1 levels and promotes amyloidogenesis. Neuron 60:988-1009.

1077 Paschen W, Mengesdorf T (2005a) Endoplasmic reticulum stress response and
1078 neurodegeneration. Cell Calcium 38:409-415.
1079 Paschen W, Mengesdorf T (2005b) Cellular abnormalities linked to endoplasmic reticulum
1080 dysfunction in cerebrovascular disease--therapeutic potential. Pharmacol Ther 108:362-
1081 375.
1082 Pozueta J, Lefort R, Shelanski ML (2013) Synaptic changes in Alzheimer's disease and its
1083 models. Neuroscience 251:51-65.
1084 Prince M WA, Guerchet M, Gemma C, Wu Tzu-Yu, Prina M (2015) World Alzheimer Report 2015
1085 - The Global Impact of Dementia: An analysis of prevalence, incidence, cost and trends.
1086 In. London.
1087 Radford H, Moreno JA, Verity N, Halliday M, Mallucci GR (2015) PERK inhibition prevents tau-
1088 mediated neurodegeneration in a mouse model of frontotemporal dementia. Acta
1089 Neuropathol 130:633-642.
1090 Ron D, Habener JF (1992) CHOP, a novel developmentally regulated nuclear protein that
1091 dimerizes with transcription factors C/EBP and LAP and functions as a dominant-negative
1092 inhibitor of gene transcription. Genes Dev 6:439-453.
1093 Ron D, Harding HP (2012) Protein-folding homeostasis in the endoplasmic reticulum and
1094 nutritional regulation. Cold Spring Harb Perspect Biol 4.
1095 Salminen A, Kauppinen A, Suuronen T, Kaarniranta K, Ojala J (2009) ER stress in Alzheimer's
1096 disease: a novel neuronal trigger for inflammation and Alzheimer's pathology. J
1097 Neuroinflamm 6.
1098 Scheper W, Hoozemans JJ (2009) Endoplasmic reticulum protein quality control in
1099 neurodegenerative disease: the good, the bad and the therapy. Curr Med Chem 16:615-
1100 626.

1101 Scheper W, Hoozemans JJ (2015) The unfolded protein response in neurodegenerative
1102 diseases: a neuropathological perspective. Acta Neuropathol 130:315-331.
1103 Schmidt EK, Clavarino G, Ceppi M, Pierre P (2009) SUnSET, a nonradioactive method to
1104 monitor protein synthesis. Nat Methods 6:275-277.
1105 Schoonenboom NS, Pijnenburg YA, Mulder C, Rosso SM, Van Elk EJ, Van Kamp GJ, Van
1106 Swieten JC, Scheltens P (2004) Amyloid beta(1-42) and phosphorylated tau in CSF as
1107 markers for early-onset Alzheimer disease. Neurology 62:1580-1584.
1108 Schroder M, Kaufman RJ (2005) The mammalian unfolded protein response. Annu Rev Biochem
1109 74:739-789.
1110 Segev Y, Barrera I, Ounallah-Saad H, Wibrand K, Sporild I, Livne A, Rosenberg T, David O,
1111 Mints M, Bramham CR, Rosenblum K (2015) PKR Inhibition Rescues Memory Deficit and
1112 ATF4 Overexpression in ApoE epsilon4 Human Replacement Mice. J Neurosci 35:12986-
1113 12993.
1114 Sekine Y, Zyryanova A, Crespillo-Casado A, Fischer PM, Harding HP, Ron D (2015) Stress
1115 responses. Mutations in a translation initiation factor identify the target of a memory-
1116 enhancing compound. Science 348:1027-1030.
1117 Selkoe DJ (2001) Alzheimer's disease: genes, proteins, and therapy. Physiol Rev 81:741-766.
1118 Shankar GM, Li S, Mehta TH, Garcia-Munoz A, Shepardson NE, Smith I, Brett FM, Farrell MA,
1119 Rowan MJ, Lemere CA, Regan CM, Walsh DM, Sabatini BL, Selkoe DJ (2008) Amyloid-
1120 beta protein dimers isolated directly from Alzheimer's brains impair synaptic plasticity and
1121 memory. Nat Med 14:837-842.
1122 Sidrauski C, McGeachy AM, Ingolia NT, Walter P (2015a) The small molecule ISRIB reverses
1123 the effects of eIF2alpha phosphorylation on translation and stress granule assembly. Elife
1124 4.

1125 Sidrauski C, Tsai JC, Kampmann M, Hearn BR, Vedantham P, Jaishankar P, Sokabe M,
1126 Mendez AS, Newton BW, Tang EL, Verschueren E, Johnson JR, Krogan NJ, Fraser CS,
1127 Weissman JS, Renslo AR, Walter P (2015b) Pharmacological dimerization and activation
1128 of the exchange factor eIF2B antagonizes the integrated stress response. Elife 4:e07314.
1129 Sidrauski C, Acosta-Alvear D, Khoutorsky A, Vedantham P, Hearn BR, Li H, Gamache K,
1130 Gallagher CM, Ang KK, Wilson C, Okreglak V, Ashkenazi A, Hann B, Nader K, Arkin MR,
1131 Renslo AR, Sonenberg N, Walter P (2013) Pharmacological brake-release of mRNA
1132 translation enhances cognitive memory. Elife 2:e00498.
1133 Sobow T, Flirski M, Liberski PP (2004) Amyloid-beta and tau proteins as biochemical markers of
1134 Alzheimer's disease. Acta Neurobiol Exp (Wars) 64:53-70.
1135 Spatara ML, Robinson AS (2010) Transgenic Mouse and Cell Culture Models Demonstrate a
1136 Lack of Mechanistic Connection Between Endoplasmic Reticulum Stress and Tau
1137 Dysfunction. J Neurosci Res 88:1951-1961.
1138 Tabas I, Ron D (2011) Integrating the mechanisms of apoptosis induced by endoplasmic
1139 reticulum stress. Nat Cell Biol 13:184-190.
1140 Takeuchi H, Iba M, Inoue H, Higuchi M, Takao K, Tsukita K, Karatsu Y, Iwamoto Y, Miyakawa T,
1141 Suhara T, Trojanowski JQ, Lee VM, Takahashi R (2011) P301S mutant human tau
1142 transgenic mice manifest early symptoms of human tauopathies with dementia and
1143 altered sensorimotor gating. Plos One 6:e21050.
1144 Terry RD, Masliah E, Salmon DP, Butters N, DeTeresa R, Hill R, Hansen LA, Katzman R (1991)
1145 Physical basis of cognitive alterations in Alzheimer's disease: synapse loss is the major
1146 correlate of cognitive impairment. Ann Neurol 30:572-580.
1147 Thomenius MJ, Distelhorst CW (2003) Bcl-2 on the endoplasmic reticulum: protecting the
1148 mitochondria from a distance. J Cell Sci 116:4493-4499.

1149 Verfaillie T, Garg AD, Agostinis P (2013) Targeting ER stress induced apoptosis and
1150 inflammation in cancer. Cancer Lett 332:249-264.
1151 Wek RC, Jiang HY, Anthony TG (2006) Coping with stress: eIF2 kinases and translational
1152 control. Biochem Soc Trans 34:7-11.
1153 West MJ, Coleman PD, Flood DG, Troncoso JC (1994) Differences in the pattern of hippocampal
1154 neuronal loss in normal ageing and Alzheimer's disease. Lancet 344:769-772.
1155 Yoshiyama Y, Higuchi M, Zhang B, Huang SM, Iwata N, Saido TC, Maeda J, Suhara T,
1156 Trojanowski JQ, Lee VM (2007) Synapse loss and microglial activation precede tangles in
1157 a P301S tauopathy mouse model. Neuron 53:337-351.
1158

**LEGENDS**

**Figure 1**: Timeline of behavioral studies conducted in PS19 and $APP^{Swe}$ mice. FC = fear conditioning, AC = activity chamber, EPM = elevated plus maze, MWM = Morris water maze, PA = passive avoidance, NOL = novel object location, NOR = novel object recognition.

**Figure 2**: Thapsigargin induced ER stress and target engagement *in vitro*. (**A**-**D**) ER stress-induced ATF4 translation, but not CHOP activation or cytotoxicity, is reduced by ISRIB in rat PCNs. **A**) Representative immunoblots of primary cortical cell lysates derived from E17 Sprague-Dawley rats probed using antibodies directed against ATF4, CHOP, and tubulin. **B**) Quantification of ATF4 levels normalized to tubulin. ATF4 is increased in cells treated with 1 μM thapsigargin or 1 μM thapsigargin + 200 nM ISRIB compared to vehicle control. Cells treated with 1 μM thapsigargin have more ATF4 compared to cells treated with 1 μM thapsigargin + 200 nM ISRIB. Vehicle, n = 6; 1 μM thapsigargin, n = 5; 1 μM thapsigargin + 200 nM ISRIB, n = 4. **C**) Quantification of CHOP levels normalized to tubulin. CHOP is increased in cells treated with 1 μM thapsigargin compared to vehicle control. Vehicle, n = 4; 1 μM thapsigargin, n = 3; 1 μM thapsigargin + 200 nM ISRIB, n = 3. **D**) Quantification of cytotoxicity by LDH. Cells treated with 10 μM thapsigargin, 10 μM thapsigargin + 200 nM ISRIB, or 10 μM thapsigargin + 1 μM ISRIB have higher percentages of cytotoxicity compared to vehicle control. Vehicle, n = 6; no vehicle, n = 6; 10 μM thapsigargin, n = 6; 10 μM thapsigargin + 200 nM ISRIB, n = 6; 10 μM thapsigargin + 1 μM ISRIB, n = 6. Error bars indicate SEM; * = $p < 0.05$, ** = $p < 0.01$, *** = $p < 0.001$, **** = $p < 0.0001$.

**Figure 3**: ER stress-related dysfunction is not observed in the $APP^{Swe}$ model *in vitro* despite evidence of ISRIB target engagement. **A**) Thapsigargin-induced ER stress is not mitigated by ISRIB in $APP^{Swe}$ mouse PCNs. Cells from nTg and Tg mice cultured for 13 DIV treated with 1 μM thapsigargin or 1 μM thapsigargin + 200 nM ISRIB have increased levels of ATF4 compared to vehicle control. nTg vehicle, n = 3; nTg + 1 μM thapsigargin, n = 3; nTg + 1 μM thapsigargin +

200 nM ISRIB, n = 3; Tg vehicle, n = 3; Tg + 1 μM thapsigargin, n = 3; Tg + 1 μM thapsigargin + 200 nM ISRIB, n = 3. **B**) Thapsigargin (1 μM) attenuates protein synthesis in nTg PCNs cultured for 7 DIV. ISRIB (200 nM) provides partial restoration of protein synthesis in PCNs challenged with thapsigargin. nTg vehicle + 10 μg/ml puromycin, n = 4; nTg + 1 μM thapsigargin + 10 μg/ml puromycin, n = 5; nTg + 1 μM thapsigargin + 200 nM ISRIB, n = 5. **C**) Thapsigargin-induced ER stress is not mitigated by ISRIB in nTg mouse PCNs. Cells from nTg mice cultured for 7 DIV treated with 1 μM thapsigargin or 1 μM thapsigargin + 200 nM ISRIB have increased levels of ATF4 compared to vehicle control. nTg vehicle, n = 6; nTg + 1 μM thapsigargin, n = 6; nTg + 1 μM thapsigargin + 200 nM ISRIB, n = 6. Error bars indicate SEM; ** = $p < 0.01$, *** $p = 0.001$, **** = $p < 0.0001$.

**Figure 4**: Peripherally administered ISRIB crosses the BBB and prolonged administration is well tolerated by C57BL/6J mice. **A**) ISRIB concentration over time in brain and plasma of 5-month-old C57BL/6J mice after a single IP injection (5 mg/kg). Plasma collected at 0.5 h (n = 4), 2 h (n = 4), 4 h (n = 3), and 8 h (n = 4) after injection. Brain tissue collected at 0.5 h (n = 4), 2 h (n = 4), 4 h (n = 4), and 8 h (n = 4) after injection. **B**) Body weights of mice receiving daily injections of vehicle or ISRIB for 9 weeks. Vehicle, n = 6; ISRIB, n = 6. **C**) Survival rates of vehicle or ISRIB-treated mice. Error bars indicate SEM.

**Figure 5**: Effects of genotype and treatment on body weight and mortality in PS19 mice. **A**) Tg mice have lower body weights compared to nTg mice. Daily administration of ISRIB reduced body weight in nTg mice over the course of 9 weeks. **B**) Tg mice have reduced survival rates compared to nTg mice. ISRIB improved survival in nTg mice. nTg vehicle, n = 27; nTg ISRIB, n = 25; Tg vehicle, n = 15; Tg ISRIB, n = 25. Asterisks (*) indicate comparisons to nTg vehicle. Error bars indicate SEM; * = $p < 0.05$, ** = $p < 0.01$, *** = $p < 0.001$, **** = $p < 0.0001$.

**Figure 6**: Despite severe behavioral impairments, ISRIB provides modest restoration of spatial acquisition deficits in PS19 Tg mice. **A**-**C**) Tg mice exhibit a characteristically hyperactive

phenotype. **A**) Quantification of ambulatory distance. Tg mice treated with ISRIB ambulate a greater distance on AC test 3 compared to nTg mice treated with ISRIB. **B**) Quantification of ambulatory duration. Tg mice treated with ISRIB spend more time moving on AC tests 2 and 3 compared to nTg mice treated with ISRIB. **C**) Quantification of rear frequency. Tg mice treated with vehicle rear more frequently on AC test 2 compared to nTg mice treated with vehicle. Tg mice treated with ISRIB rear more frequently on AC tests 3 and 4 compared to nTg mice treated with ISRIB. nTg vehicle, n = 27; nTg ISRIB, n = 25; Tg vehicle, n = 25; Tg ISRIB, n = 25. **D**) Tg mice exhibit diminished anxiety-like behavior. Tg mice treated with vehicle or ISRIB spend more time in the open arms of the EPM compared to nTg mice treated with vehicle. nTg vehicle, n = 26; nTg ISRIB, n = 25; Tg vehicle, n = 24; Tg ISRIB, n = 22. **E-G**) Tg mice display impaired spatial learning and memory with modest restoration of acquisition by ISRIB. **E**) Quantification of escape latency during the acquisition/training phase of the MWM. Tg mice treated with vehicle took longer to locate the platform on each day compared to nTg mice treated with vehicle. Tg mice treated with ISRIB took longer to locate the platform on days 1 and 2 compared to nTg mice treated with vehicle. Tg mice treated with ISRIB took longer to locate the platform on day 2 compared to nTg mice treated with ISRIB. All groups located the platform significantly faster on days 2-5 compared to day 1. **F, G**) Quantification of quadrant duration during the MWM probe test conducted 24 h and 72 h after training. nTg mice treated with vehicle or ISRIB spent significantly more time in the target quadrant compared to the nontarget quadrant during the 24 h (**F**) and 72 h (**G**) probe tests. nTg vehicle, n = 23; nTg ISRIB, n = 24; Tg vehicle, n = 15; Tg ISRIB, n = 12. **H**) Tg mice do not exhibit fear-based associative learning and memory deficit. Quantification of latency to cross during the habituation, training, and testing phases of the passive PA test are shown. All groups took significantly longer to cross during testing compared to the training phase. nTg vehicle, n = 24; nTg ISRIB, n = 23; Tg vehicle, n = 17; Tg ISRIB, n = 17. Asterisks (*) indicate comparisons to nTg vehicle; $ indicate comparisons to nTg ISRIB; #

indicate within group comparisons to trial 1. Error bars indicate SEM; $, * = $p < 0.05$; $$, ** = $p < 0.01$, *** = $p < 0.001$; #, **** = $p < 0.0001$.

**Figure 7**: ER stress does not appear to be implicated in PS19 Tg neuropathology. **A**) Representative immunoblot of cortical tissue lysate from nTg and Tg mice probed using antibodies directed against ATF4 and CHOP. CHOP was detected only in PCN lysate derived from E17 Sprague-Dawley rats treated with 1 μM thapsigargin, which served as a positive control (+ control). **B**) Quantification of ATF4 normalized to tubulin. No significant differences in levels of ATF4 were found. nTg vehicle, n = 12; nTg ISRIB, n = 15; Tg vehicle, n = 6; Tg ISRIB, n = 8; + control (n = 2). **C**) Representative immunoblot of hippocampal tissue lysate from nTg and Tg mice probed using antibodies directed against p-tau (AT8) and total tau (Tau5). **D**) Quantification of AT8 normalized to Tau5 and Tau5 normalized to GAPDH. Tg mice treated with ISRIB have significantly more AT8 compared to Tg mice treated with vehicle. Tg + vehicle, n = 6; Tg + ISRIB, n = 8. Error bars indicate SEM; * = $p < 0.05$.

**Figure 8**: PS19 Tg mice have increased p-tau and evidence of hippocampal degeneration. **A**) Representative photomicrographs (5x) of the hippocampus in nTg and Tg mice treated with vehicle or ISRIB. Sections stained using DAPI, fluoro-nissl, and antibody directed at p-tau (AT8). Boxes indicate the ROIs. **B**) Representative photomicrographs (40x) of the endal limb of the DG in nTg and Tg mice treated with vehicle or ISRIB. Sections stained using DAPI, fluoro-nissl, and antibody directed at p-tau (AT8). **C**) Quantification of AT8 in the DG. Tg mice treated with ISRIB have an increased number of p-tau immunoreactive inclusions in the DG compared to nTg mice treated with vehicle. Error bars indicate SEM; * = $p < 0.05$. **D**) Quantification of AT8 in the hippocampus. Tg mice have an increased number of p-tau immunoreactive inclusions throughout CA1, CA3, and the DG compared to nTg mice treated with vehicle. Error bars indicate SEM; ** = $p < 0.01$. **E**) Representative photomicrographs (2.5x) of brain sections from nTg and Tg mice treated with vehicle or ISRIB. Arrows indicate the pyramidal cell layer of CA1.

Sections stained using fluoro-nissl. **F**) Quantification of CA1 layer thickness. Tg mice have significant reductions in CA1 compared to nTg mice treated with vehicle. nTg vehicle, n = 7; nTg ISRIB, n = 7; Tg vehicle, n = 7; Tg ISRIB, n = 7. Error bars indicate SD; ** = $p < 0.01$.

**Figure 9**: Effects of genotype and treatment on body weight and mortality in $APP^{Swe}$ mice. **A**) Tg mice have reductions in body weight compared to nTg mice. **B**) ISRIB reduced survival in nTg and Tg mice by the 8th day of treatment. nTg vehicle, n = 14; nTg ISRIB, n = 15; Tg vehicle, n = 15; Tg ISRIB, n = 14. Asterisks (*) indicate comparisons to nTg vehicle; # indicate comparisons to Tg vehicle. Error bars indicate SEM; * = $p < 0.05$; #, ** = $p < 0.01$.

**Figure 10**: $APP^{Swe}$ Tg mice exhibit learning and memory deficits and behavioral impairments. **A**, **B**) Tg mice display locomotor hyperactivity. **A**) Quantification of ambulatory distance. Tg mice treated with ISRIB ambulate a greater distance compared to nTg mice treated with ISRIB. **B**) Quantification of ambulatory duration in center. Tg mice spend more time in the center of the AC compared to nTg mice treated with vehicle. nTg vehicle, n = 14; nTg ISRIB, n = 13 (n = 15 for center duration); Tg vehicle, n = 14; Tg ISRIB, n = 14. **C**, **D**) Tg mice exhibit deficits in fear-based learning and memory. **C**) Quantification of freezing behavior during the acquisition phase of the fear conditioning paradigm. Tg mice treated with ISRIB freeze less during tone 2 compared to nTg mice treated with ISRIB. During ITI2, Tg mice treated with vehicle or ISRIB freeze less compared to nTg mice treated with vehicle, and Tg mice treated with ISRIB freeze less compared to nTg mice treated with ISRIB. **D**) Quantification of freezing behavior during context- or cue-based retrieval. Tg mice freeze significantly less compared to nTg mice treated with vehicle during context-based retrieval. No significant differences were found in time spent freezing to tone. nTg vehicle, n = 14; nTg ISRIB, n = 15; Tg vehicle, n = 15; Tg ISRIB, n = 14. Asterisks (*) indicate comparisons to nTg vehicle, $ indicate comparisons to nTg ISRIB. **E**, **F**) Tg mice do not display deficits in spatial learning and memory. **E**) Quantification of escape latency during the second MWM acquisition phase and reversal trial (inset). nTg mice treated with

vehicle located the platform significantly faster on day 5 compared to day 1. Tg mice treated with vehicle located the platform significantly faster on days 3, 4, and 5 compared to day 1. nTg mice treated with vehicle and Tg mice treated with vehicle or ISRIB took longer to locate the platform on the reversal trial (see inset) compared to day 5. Additional between group comparisons were made for each training day and no significant differences were found. # indicates comparisons made within group to trial 1. **F**) Quantification of escape latency during the second MWM probe trial. All groups spent significantly more time in the target quadrant compared to the nontarget quadrant. nTg vehicle, n = 10; nTg ISRIB, n = 4; Tg vehicle, n = 11; Tg ISRIB, n = 6. **G, H**) Tg mice exhibit phenotypic deficits in spatial working memory and short-term recognition memory. **G**) Quantification of percent alternation during the Y-maze. nTg mice treated with vehicle had a significantly greater percent alternation compared to 50% chance alternation. No significant differences were found between groups in total number of entries or percentage of correct entries in the Y-maze (data not shown). nTg vehicle, n = 14; nTg ISRIB, n = 11; Tg vehicle, n = 15; Tg ISRIB, n = 10. **H**) Quantification of percentage of time spent investigating the novel or familiar object during the novel object recognition test. nTg mice treated with vehicle spent more time investigating the novel object compared to the familiar object. nTg vehicle, n = 12; nTg ISRIB, n = 10; Tg vehicle, n = 15; Tg ISRIB, n = 10. Error bars indicate SEM; #, * = $p < 0.05$; ##, $$, ** = $p < 0.01$, *** = $p < 0.001$; $$$$, **** = $p < 0.0001$.

**Table 1**: Total number, genotype, and age of mice used for the present studies are shown.

**Table 2**: A summary of the statistical tests used for analyses and corresponding figure(s).

**Table 3**: A summary of the results of the behavioral outcomes used for phenotype analysis in PS19 mice are provided. Comparisons made to nTg vehicle control. AC = activity chamber, EPM = elevated plus maze, MWM = Morris water maze, D1-5 = Day 1-5, PA = passive avoidance.

**Table 4**: A summary of the results of the behavioral outcomes used for phenotype analysis in $APP^{Swe}$ mice are provided above. Comparisons made to nTg vehicle control. AC = activity

chamber, ITI = inter-trial interval, MWM = Morris water maze, D1-5 = Day 1-5, R = reversal trial, NOR = novel object recognition.

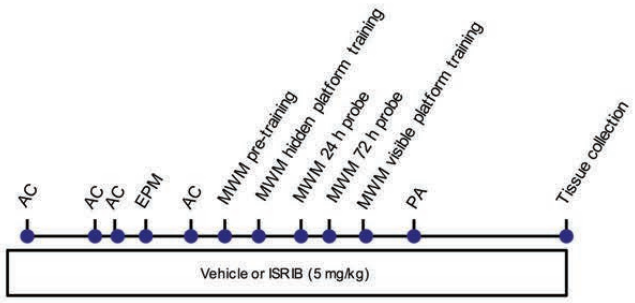


**PS19 age (mo)** 8.0 8.5 9.0 9.5 10.0 10.5 11.0

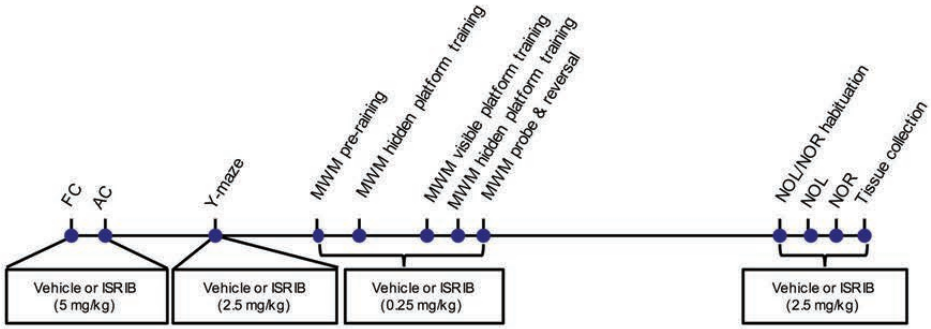


**APP$^{Swe}$ age (mo)** 5.0 5.5 6.0 6.5 7.0 7.5 8.0

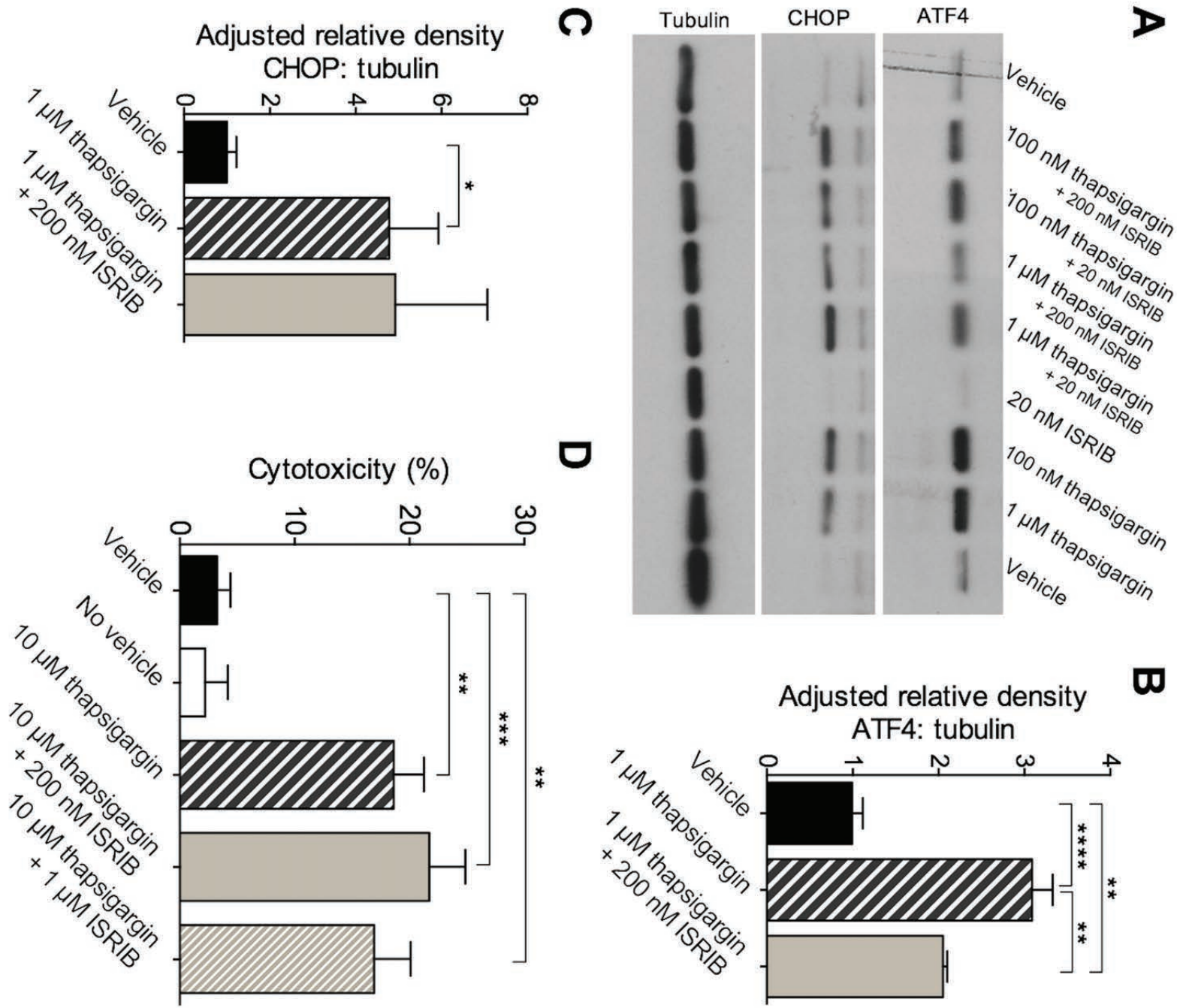

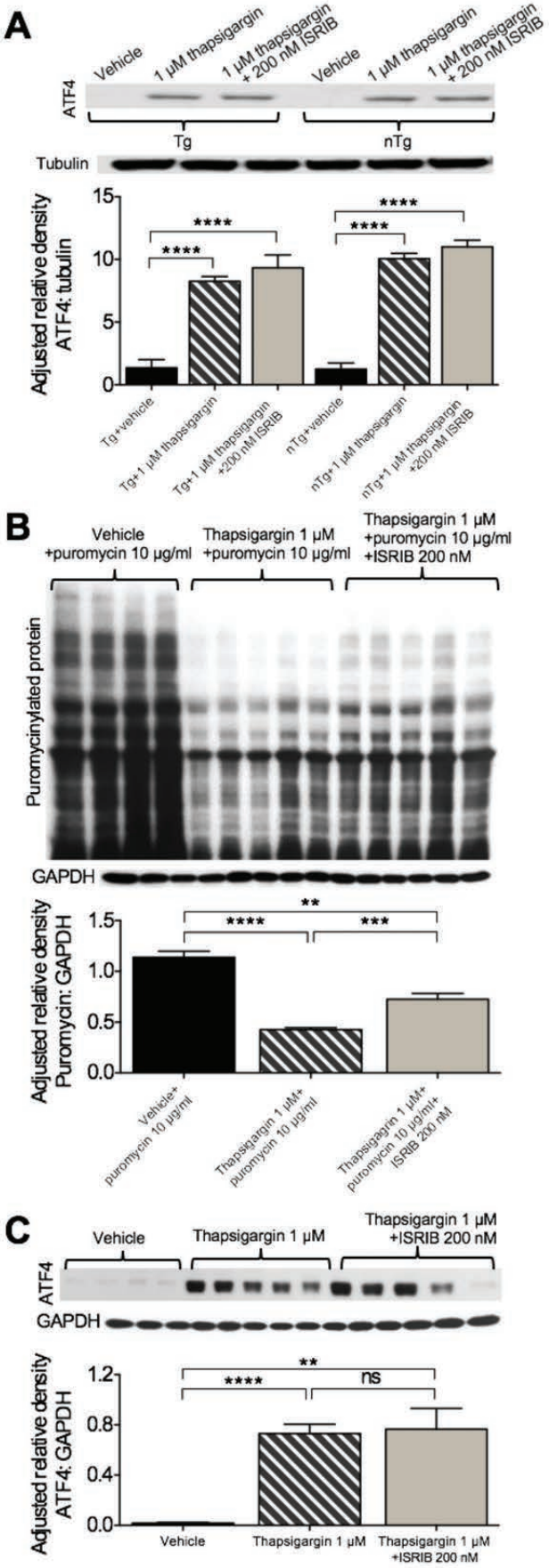

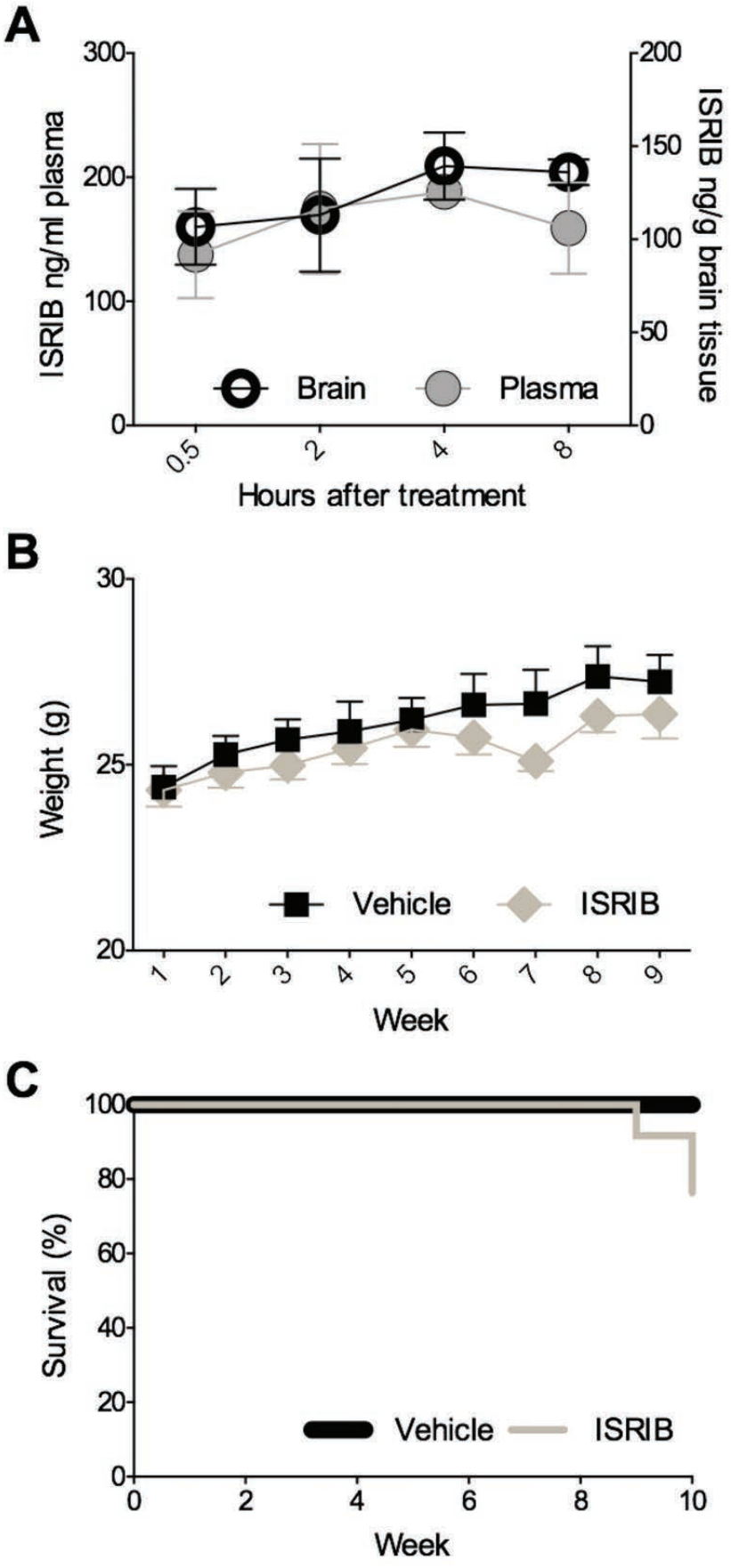

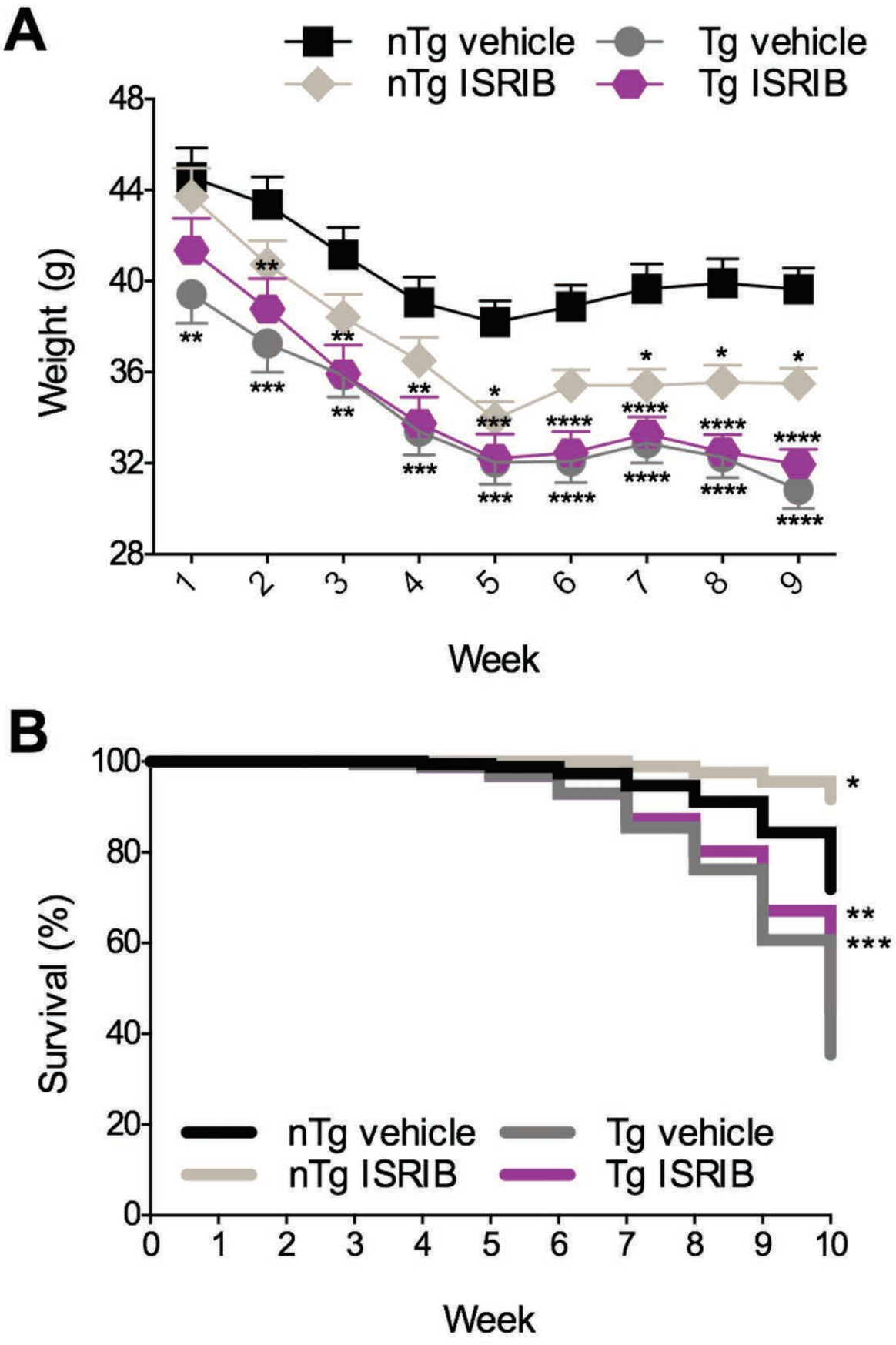

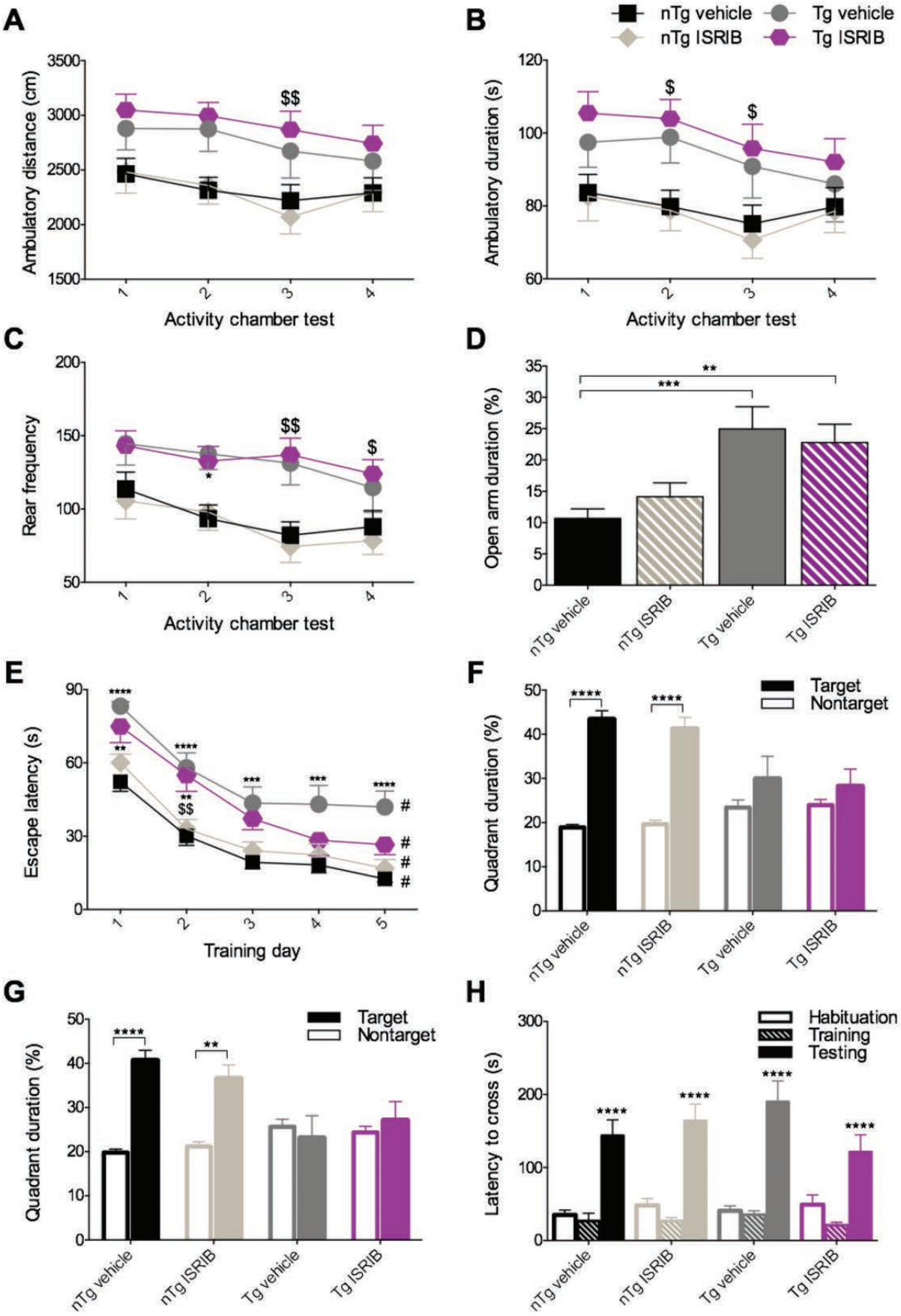

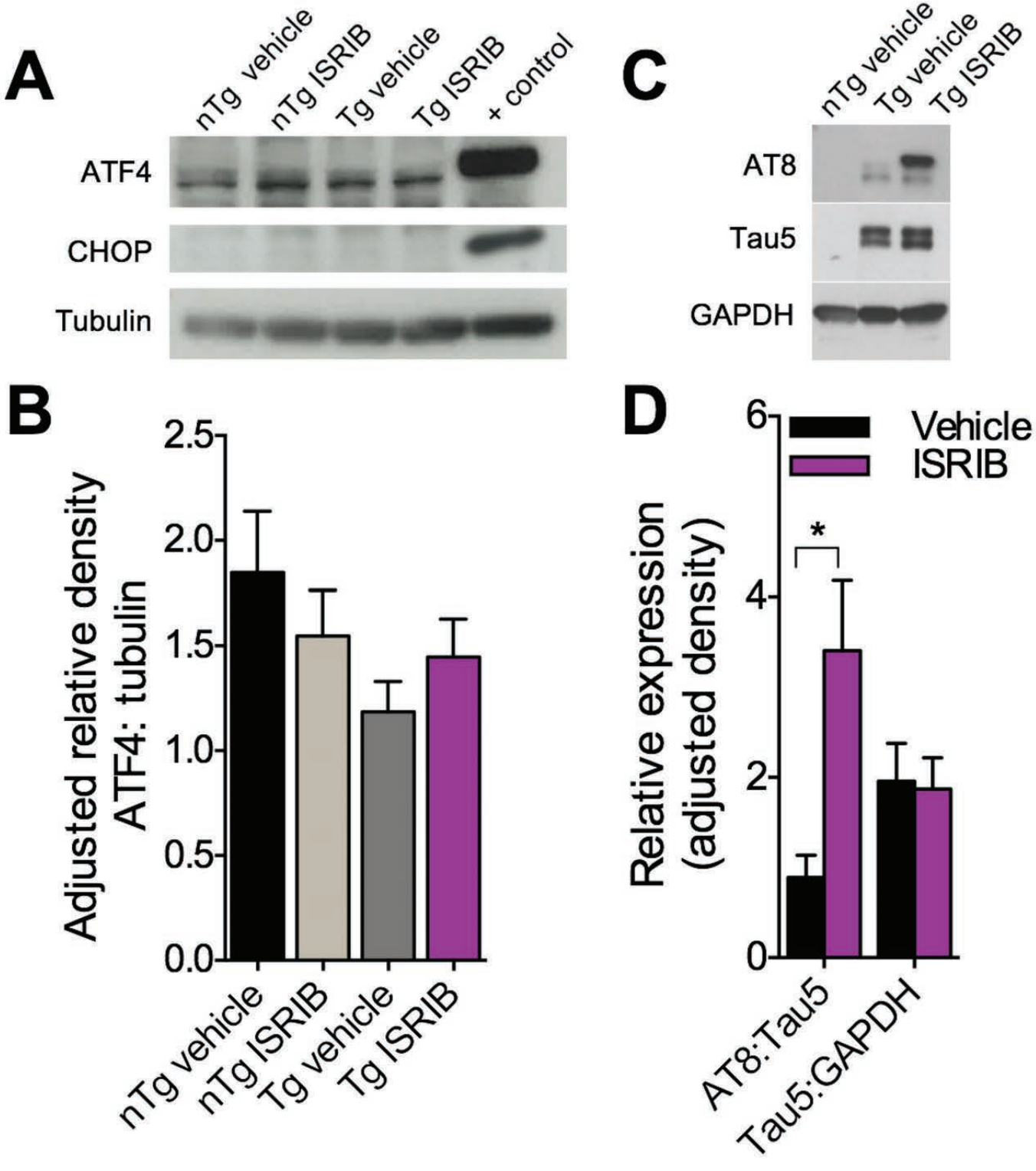

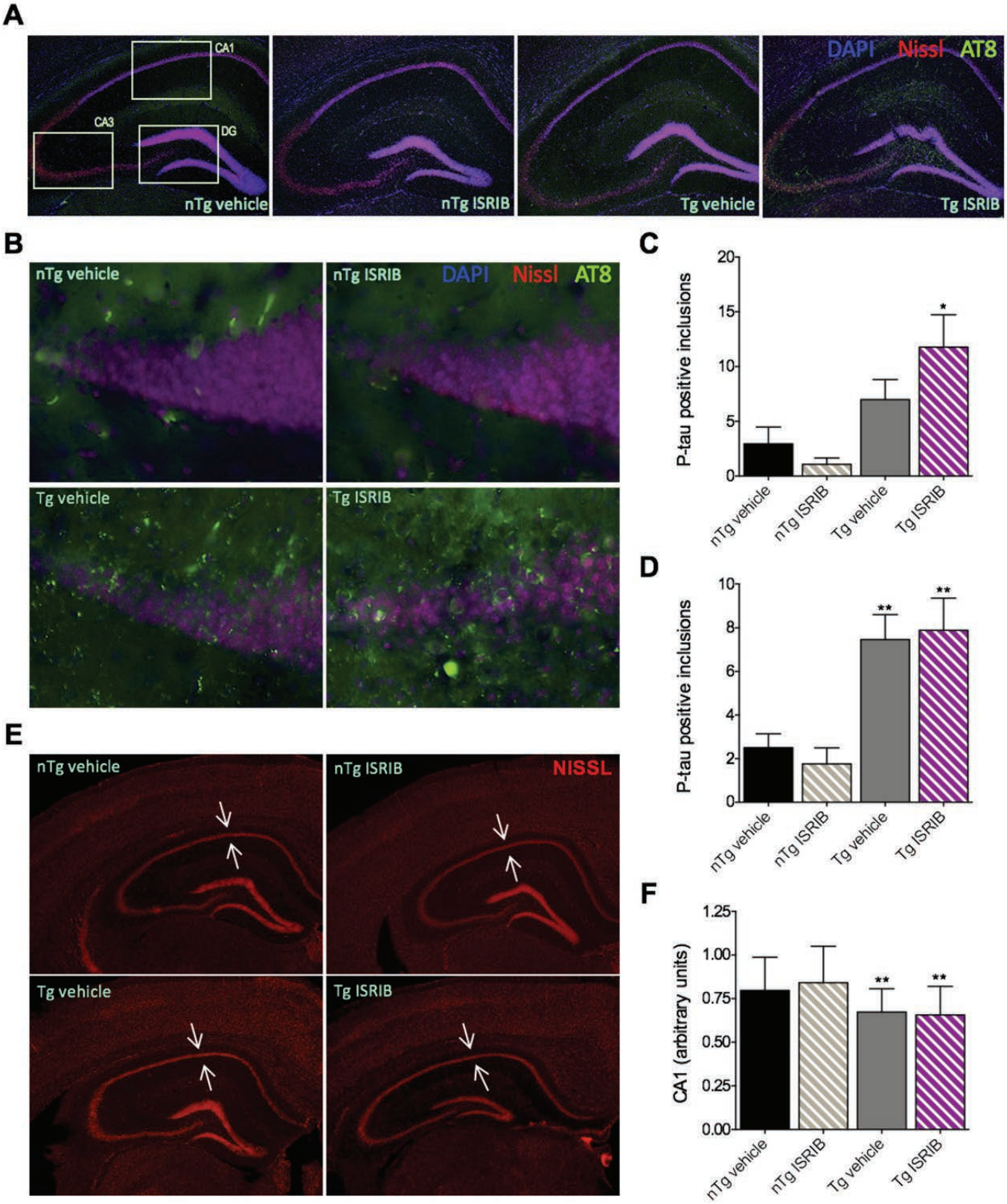

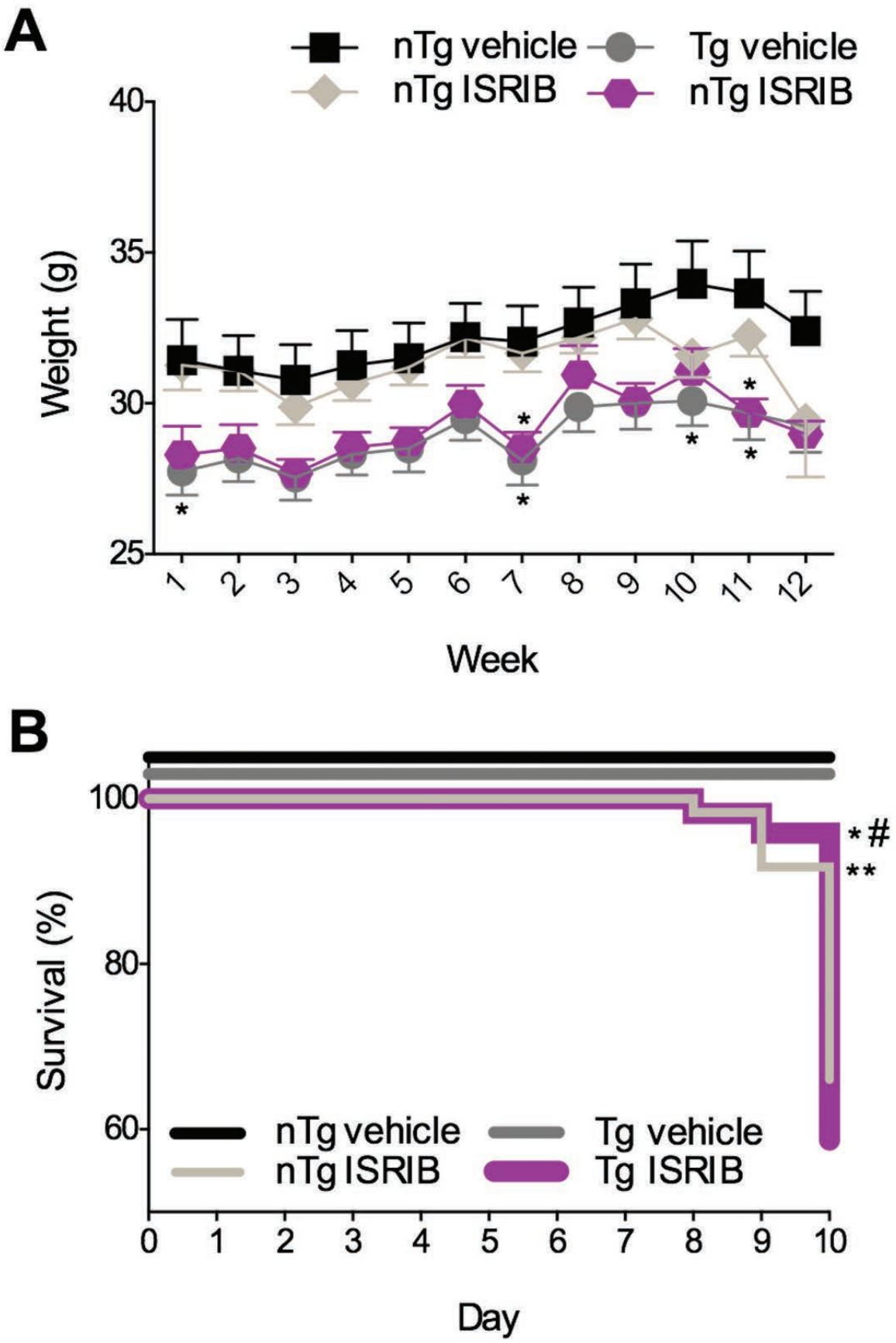

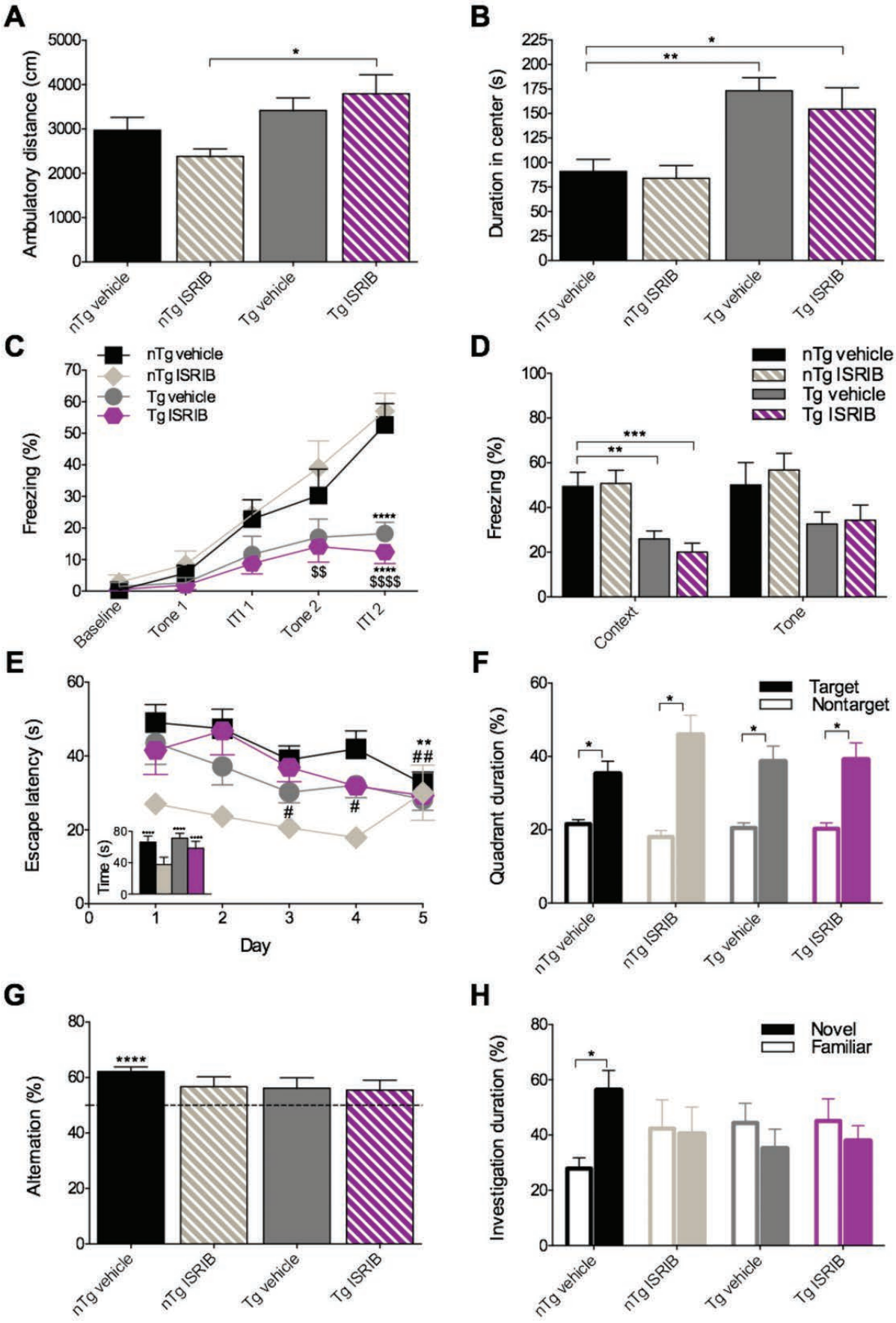

**Table 1**: Summary of mice used for the present studies

| | C57BL/6J | C57BL/6J | PS19 | $APP^{Swe}$ |
|---|---|---|---|---|
| Age (months) | 3 | 5 | 8-9 | 5-6 |
| N | 20 | 12 | 102 | 60 |

**Table 2**: Statistical tests used for analyses

| Figure | Statistical test used for analysis |
|---|---|
| Fig. 2B: ATF4 in rat PCNs<br>Fig. 2D: LDH in rat PCNs<br>Fig. 3A, 3C: ATF4 in $APP^{Swe}$ PCNs<br>Fig. 6D: Anxiety-like behavior in PS19 mice<br>Fig. 6H: Fear-based learning & memory in PS19 mice<br>Fig. 7B: ATF4 in PS19 mice<br>Fig. 8C,D P-tau by IHC in PS19 mice<br>Fig. 8F: CA1 pyramidal cell layer in PS19 mice<br>Fig. 10A,B: Locomotor activity in $APP^{Swe}$ mice<br>Fig. 10D: Fear-based retrieval in $APP^{Swe}$ mice | One-way ANOVA;<br>Bonferroni's MCT |
| Fig. 2C: CHOP in rat PCNs<br>Fig. 3B: SUnSET<br>Fig. 3C: ATF4 in mouse PCNs<br>Fig. 6F,G: MWM spatial memory recall in PS19 mice<br>Fig. 7D: Tau by immunoblot in PS19 mice<br>Fig. 10F: MWM spatial memory recall in $APP^{Swe}$ mice<br>Fig. 10G: Exploratory behavior in $APP^{Swe}$ mice<br>Fig. 10H: Recognition memory in $APP^{Swe}$ mice<br>Tables 3 & 4: Phenotype analysis | T-tests (Student's, one-sample, paired samples) |
| Fig. 4A: PK | Two-way ANOVA<br>Linear regression |
| Fig. 4B: Body weight in C57BL/6J mice<br>Fig. 6A-C: Locomotor activity in PS19 mice<br>Fig. 6E: MWM spatial acquisition in PS19 mice<br>Fig. 5A: Body weight in PS19 mice<br>Fig. 9A: Body weight in $APP^{Swe}$ mice<br>Fig. 10C: Fear conditioning in $APP^{Swe}$ mice<br>Fig. 10E: MWM spatial acquisition in $APP^{Swe}$ mice | Two-way RM or mixed-measures ANOVA; Bonferroni's MCT |
| Fig. 4C: Survival rate in C57BL/6J mice<br>Fig. 5B: Survival rate in PS19 mice<br>Fig. 9B: Survival rate in $APP^{Swe}$ mice | Mantel-Cox |

**Table 3**: Summary of behavioral outcomes for phenotype analysis of PS19 mice

| Behavior | Test | Dependent variable | Genotype | Treatment | Mean±SEM | *p* value | Interpretation |
|---|---|---|---|---|---|---|---|
| Locomotion | AC 1 | Ambulatory distance (cm) | PS19 nTg | Vehicle | 83.64±5.01 | - | PS19 Tg mice display a hyperactive phenotype evidenced by increased locomotor activity |
| | | | | ISRIB | 97.50±6.89 | ns | |
| | | | PS19 Tg | Vehicle | 82.65±6.73 | ns | |
| | | | | ISRIB | 105.48±5.87 | ns | |
| | AC 2 | Ambulatory distance (cm) | PS19 nTg | Vehicle | 79.88±4.43 | - | |
| | | | | ISRIB | 78.79±5.60 | ns | |
| | | | PS19 Tg | Vehicle | 98.85±7.06 | ns | |
| | | | | ISRIB | 103.98±5.26 | $p < 0.05$ | |
| | AC 3 | Ambulatory distance (cm) | PS19 nTg | Vehicle | 75.09±5.16 | - | |
| | | | | ISRIB | 70.62±4.98 | ns | |
| | | | PS19 Tg | Vehicle | 90.88±8.72 | ns | |
| | | | | ISRIB | 95.82±6.62 | $p < 0.05$ | |
| | AC 4 | Ambulatory distance (cm) | PS19 nTg | Vehicle | 79.78±5.28 | - | |
| | | | | ISRIB | 78.59±5.85 | ns | |
| | | | PS19 Tg | Vehicle | 86.06±10.40 | ns | |
| | | | | ISRIB | 92.07±6.42 | ns | |
| Anxiety-like behavior | EPM | Open arm duration (%) | PS19 nTg | Vehicle | 10.67±1.55 | - | PS19 Tg mice exhibit reduced anxiety-like behavior |
| | | | | ISRIB | 14.14±2.23 | ns | |
| | | | PS19 Tg | Vehicle | 24.99±3.53 | $p < 0.001$ | |
| | | | | ISRIB | 22.80±2.91 | $p < 0.01$ | |
| Spatial acquisition learning | MWM D1 | Escape latency (s) | PS19 nTg | Vehicle | 52.26±3.86 | - | PS19 Tg mice display impairments in spatial learning with modest restoration by ISRIB |
| | | | | ISRIB | 60.11±3.52 | ns | |
| | | | PS19 Tg | Vehicle | 83.22±1.94 | $p < 0.0001$ | |
| | | | | ISRIB | 74.89±6.55 | $p < 0.01$ | |
| | MWM D2 | | PS19 nTg | Vehicle | 30.15±3.90 | - | |
| | | | | ISRIB | 33.01±3.89 | ns | |
| | | | PS19 Tg | Vehicle | 58.06±6.04 | $p < 0.0001$ | |
| | | | | ISRIB | 55.05±6.61 | $p < 0.01$ | |
| | MWM D3 | | PS19 nTg | Vehicle | 19.38±2.50 | - | |
| | | | | ISRIB | 24.03±3.61 | ns | |
| | | | PS19 Tg | Vehicle | 43.58±6.60 | $p < 0.0001$ | |
| | | | | ISRIB | 37.15±4.50 | ns | |
| | MWM D4 | | PS19 nTg | Vehicle | 18.32±3.21 | - | |
| | | | | ISRIB | 22.36±4.50 | ns | |
| | | | PS19 Tg | Vehicle | 43.08±7.72 | $p < 0.001$ | |
| | | | | ISRIB | 28.38±6.16 | ns | |
| | MWM D5 | | PS19 nTg | Vehicle | 12.56±1.32 | - | |
| | | | | ISRIB | 16.87±3.59 | ns | |
| | | | PS19 Tg | Vehicle | 41.98±6.54 | $p < 0.0001$ | |
| | | | | ISRIB | 26.54±4.04 | ns | |
| Spatial memory recall | Prove test 24 h | Quadrant duration (%) | PS19 nTg | Vehicle | -24.45±2.71 | $p < 0.0001$ | PS19 Tg mice display impaired spatial memory recall |
| | | | | ISRIB | -21.54±3.55 | $p < 0.0001$ | |
| | | | PS19 Tg | Vehicle | -6.43±6.89 | ns | |
| | | | | ISRIB | -4.26±5.28 | ns | |
| | Prove test 72 h | | PS19 nTg | Vehicle | -20.84±3.07 | $p < 0.0001$ | |
| | | | | ISRIB | -15.33±4.20 | $p < 0.01$ | |
| | | | PS19 Tg | Vehicle | 2.57±6.76 | ns | |
| | | | | ISRIB | -2.76±5.70 | ns | |
| Fear learning & memory | PA: training vs testing | Latency to cross (s) | PS19 nTg | Vehicle | 117±22 | $p < 0.0001$ | PS19 Tg mice do not exhibit deficits in fear-based learning and memory |
| | | | | ISRIB | 137±24 | $p < 0.0001$ | |
| | | | PS19 Tg | Vehicle | 155±28 | $p < 0.0001$ | |
| | | | | ISRIB | 100±22 | $p < 0.001$ | |

**Table 4**: Summary of behavioral outcomes for phenotype analysis of $APP^{Swe}$ mice

| Behavior | Test | Dependent variable | Genotype | Treatment | Mean±SEM | *p* value | Interpretation |
|---|---|---|---|---|---|---|---|
| Locomotion | AC | Ambulatory distance (cm) | $APP^{Swe}$ nTg | Vehicle | 108.20±9.45 | - | $APP^{Swe}$ Tg mice exhibit locomotor hyperactivity |
| | | | | ISRIB | 88.75±6.40 | ns | |
| | | | $APP^{Swe}$ Tg | Vehicle | 124.80±9.78 | ns | |
| | | | | ISRIB | 139.50±15.10 | ns | |
| | | Center duration (s) | $APP^{Swe}$ nTg | Vehicle | 90.97±12.30 | - | |
| | | | | ISRIB | 83.92±13.13 | ns | |
| | | | $APP^{Swe}$ Tg | Vehicle | 173.40±13.15 | $p < 0.01$ | |
| | | | | ISRIB | 154.50±21.89 | $p < 0.05$ | |
| Fear-associated learning | Baseline | Freezing (%) | $APP^{Swe}$ nTg | Vehicle | 0.38±0.23 | - | $APP^{Swe}$ Tg mice display impairments in fear-associated learning |
| | | | | ISRIB | 2.82±2.34 | ns | |
| | | | $APP^{Swe}$ Tg | Vehicle | 1.50±1.26 | ns | |
| | | | | ISRIB | 0.57±0.37 | ns | |
| | Tone 1 | | $APP^{Swe}$ nTg | Vehicle | 5.69±2.33 | - | |
| | | | | ISRIB | 8.43±4.31 | ns | |
| | | | $APP^{Swe}$ Tg | Vehicle | 2.72±1.61 | ns | |
| | | | | ISRIB | 1.90±1.39 | ns | |
| | ITI1 | | $APP^{Swe}$ nTg | Vehicle | 22.83±6.21 | - | |
| | | | | ISRIB | 24.18±4.67 | ns | |
| | | | $APP^{Swe}$ Tg | Vehicle | 11.62±5.76 | ns | |
| | | | | ISRIB | 8.79±3.27 | ns | |
| | Tone 2 | | $APP^{Swe}$ nTg | Vehicle | 30.36+8.32 | - | |
| | | | | ISRIB | 39.02±8.62 | ns | |
| | | | $APP^{Swe}$ Tg | Vehicle | 17.13±5.71 | ns | |
| | | | | ISRIB | 14.15±4.93 | ns | |
| | ITI2 | | $APP^{Swe}$ nTg | Vehicle | 52.64+6.80 | - | |
| | | | | ISRIB | 60.00±5.69 | ns | |
| | | | $APP^{Swe}$ Tg | Vehicle | 18.26±3.56 | $p < 0.0001$ | |
| | | | | ISRIB | 12.42±3.62 | $p < 0.0001$ | |
| Fear-based retrieval | Context-based | | $APP^{Swe}$ nTg | Vehicle | 49.45±6.35 | - | APPSwe Tg exhibit impaired context-based fear memory retrieval |
| | | | | ISRIB | 50.76±5.95 | ns | |
| | | | $APP^{Swe}$ Tg | Vehicle | 25.93±3.63 | $p < 0.01$ | |
| | | | | ISRIB | 20.10±4.03 | $p < 0.001$ | |
| | Cue-based | | $APP^{Swe}$ nTg | Vehicle | 50.12±10.06 | - | $APP^{Swe}$ Tg mice do not display impairments in cue-based fear memory retrieval |
| | | | | ISRIB | 56.82±7.39 | ns | |
| | | | $APP^{Swe}$ Tg | Vehicle | 32.64±5.32 | ns | |
| | | | | ISRIB | 34.35±6.74 | ns | |
| Spatial acquisition learning | MWM D1 | Escape latency (s) | $APP^{Swe}$ nTg | Vehicle | 33.10±4.88 | ns | $APP^{Swe}$ Tg do not exhibit impairments in spatial memory acquisition |
| | | | | ISRIB | 16.08±3.15 | ns | |
| | | | $APP^{Swe}$ Tg | Vehicle | 32.56±5.84 | ns | |
| | | | | ISRIB | 24.57±6.55 | ns | |
| | MWM D2 | | $APP^{Swe}$ nTg | Vehicle | 31.44±5.30 | ns | |
| | | | | ISRIB | 12.66±2.79 | ns | |
| | | | $APP^{Swe}$ Tg | Vehicle | 26.21±5.01 | ns | |
| | | | | ISRIB | 29.79±6.50 | ns | |
| | MWM D3 | | $APP^{Swe}$ nTg | Vehicle | 23.02±3.74 | ns | |
| | | | | ISRIB | 9.58±1.93 | ns | |
| | | | $APP^{Swe}$ Tg | Vehicle | 19.19±2.90 | ns | |
| | | | | ISRIB | 19.92±3.92 | ns | |
| | MWM D4 | | $APP^{Swe}$ nTg | Vehicle | 25.95±4.86 | ns | |
| | | | | ISRIB | 6.91±1.21 | ns | |
| | | | $APP^{Swe}$ Tg | Vehicle | 21.12±3.41 | ns | |
| | | | | ISRIB | 14.86±1.82 | ns | |
| | MWM D5 | | $APP^{Swe}$ nTg | Vehicle | 16.56±3.15 | $p < 0.01$ | |
| | | | | ISRIB | 19.04±7.50 | ns | |
| | | | $APP^{Swe}$ Tg | Vehicle | 17.29±2.99 | ns | |
| | | | | ISRIB | 12.30±1.49 | ns | |
| | MWM R | | $APP^{Swe}$ nTg | Vehicle | 66.35±7.55 | $p < 0.0001$ | |
| | | | | ISRIB | 37.79±9.25 | ns | |
| | | | $APP^{Swe}$ Tg | Vehicle | 71.21±6.16 | $p < 0.0001$ | |
| | | | | ISRIB | 58.59±8.69 | $p < 0.0001$ | |
| Spatial memory recall | Probe test | Duration (%) | $APP^{Swe}$ nTg | Vehicle | -13.65±4.63 | $p < 0.05$ | $APP^{Swe}$ Tg display intact spatial memory recall |
| | | | | ISRIB | -27.80±7.17 | $p < 0.05$ | |
| | | | $APP^{Swe}$ Tg | Vehicle | -18.06±5.72 | $p < 0.05$ | |
| | | | | ISRIB | -18.74±6.18 | $p < 0.05$ | |
| Working memory | Y-maze | Alternation (%) | $APP^{Swe}$ nTg | Vehicle | 62.17±1.71 | $p < 0.0001$ | $APP^{Swe}$ Tg mice display impaired working memory |
| | | | | ISRIB | 56.77±3.52 | ns | |
| | | | $APP^{Swe}$ Tg | Vehicle | 56.23±3.71 | ns | |
| | | | | ISRIB | 55.46±3.61 | ns | |
| Recognition memory | NOR | Duration (%) | $APP^{Swe}$ nTg | Vehicle | -28.39±10.47 | $p < 0.05$ | $APP^{Swe}$ Tg exhibit deficits |
| | | | | ISRIB | 1.95±19.43 | ns | |

| | | | | | | | |
|---|---|---|---|---|---|---|---|
| | | | $APP^{Swe}$ Tg | Vehicle | 9.34±13.48 | ns | in recognition memory |
| | | | | ISRIB | 7.32±12.88 | ns | |